Bachelor Project

Czech Technical University in Prague

F3

Faculty of Electrical Engineering
Department of Electromagnetic Field

Quantum Mechanical study of electronic properties of systems derived from transition metal dichalcogenides

Marek Hulec

Supervisor: Antonio Cammarata, PhD.
Field of study: Electronics and communications
July 2021

Acknowledgements

I would like to thank Antonio Cammarata, PhD., for his guidance, valuable time, and patience.

Declaration

I declare that this work is all my own and I have cited all the sources I have used in the bibliography.

Prague, July 30, 2021

Prohlašuji, že jsem předloženou práci vypracoval samostatně, a že jsem uvedl veškerou použitou literaturu.

V Praze, 30. července 2021

Abstract

The increasing energy demand and the pressure for a sustainable development impose the transition to carbon-neutral power generation. Photovoltaic solar cells are at the forefront of the transition, and improvement of their efficiency requires going beyond the standard technologies. Among the different proposed solutions, few-layered transition metal dichalcogenides (TMDs) show the ideal characteristics and might, ultimately, substitute the conventional cells.

The present work is inserted into this perspective. By means of quantum mechanical approaches we study how to engineer the electronic band gap in two- and three-layered transition metal dichalcogenides. To this aim, we investigate on the effect that the cation substitution has onto the electronic structure. We determine that the number of layers (geometric factor) and the kind of anion forming the structure (electronic factor) play the major role in the determination of the width of the band gap. Instead, the kind of dopant and its position within the layered environment might serve as a "knob" to fine tune the final value of the gap. Interestingly, we observe that, when the tellurium anion is present in the structure, the effect of the dopant is mitigated.

These preliminary results constitute the starting point of a future work in which more detailed analyses will be performed; such work will identify the guidelines for the selection of suitable dopants and local geometrical arrangements to achieve targeted values of the electronic band gap in TMD-based photovoltaic cells.

Keywords: few-layered transition metal dichalcogenides, ab initio, Density Functional Theory, band gap tuning, doping

Supervisor: Antonio Cammarata, PhD.
Advanced Materials Group,
Department of Control Engineering,
Faculty of Electrical Engineering,
Czech Technical University in Prague
Prague, Czech Republic

Abstrakt

Rastúci dopyt po energií a tlak na udržateľný rozvoj vyžadujú prechod na ulhlíkovo neutrálnu výrobu elektrickej energie. Fotovoltaické články sú napopredí tohto prechodu. Zvýšenie ich efektivity vyžaduje hľadanie riešení nad rámec štandardných technológií. Okrem iných navrhovaných alternatív niekoľkovrstvové dichalkogenidy prechodných kovov (DPK) majú ideálne vlastnosti na tento účel a napokon môžu nahradiť konvenčné solárne články.

Nasledujúca štúdia je realizovaná v rámci tejto perspektívy. Za pomoci kvantovej mechaniky sú skúmané možnosti úpravy šírky zakázaného pásu dvoj a troj vrstvých DPK. Preto sme skúmali efekt katiónovej substitúcie na elektrónovú pásovú štruktúru. Bolo zistené, že počet vrstiev a typ aniónu v štruktúre majú najväčší vplyv na šírku zakázaného pásu. Naopak, typ dopantu a jeho pozícia v určitej vrstve sa dá použiť na jemné ladenie šírky pásu. Zaujímavé je, že prítomnosť aniónu telúru v štruktúre spôsobí potlačenie efektov dopantu.

Na týchto predbežných výsledkoch bude stavať nasledujúca práca s detailnejšími analýzami. Výstupom práce budú konkrétkne spôsoby získania vybraných šíriek zakázaného pásu vo fotovoltaických článkoch založených na DPK buď výberom určitých dopantov alebo zmenou geometrického usporiadania.

Klíčová slova: niekoľkovrstvové dichalkogenidy prechodných kovov, ab initio, teória funkcionálu hustoty, ladenie zakázaného pásu, doping

Překlad názvu: Kvantově-mechanická studie elektronických vlastností systémů odvozených od dichalkogenidů přechodných kovů

Contents

Figures

Tables

Chapter 1

Introduction

Based on the statistics provided by NASA, 2016 and 2020 were the warmest years on record since 1880 [3]. Furthermore, carbon dioxide emissions have increased by 170% from before 1850 [4]. In 2016, 73% of greenhouse gasses were generated by energy production [5], while in 2019 renewable energy sources comprised about 27% of the total electricity production [6]. To counter the effects of climate change, the European Union has created a vision of a carbon-neutral economy by 2050 [7], and an energy transition to carbon-neutral power generation is proposed [8]. Renewable energy sources play a major role in the transition. Wind energy is a mature technology which is thought to become the primary source of power in the EU by 2030 supplying about 30% of the total energy production [8]. Geothermal power generation is another well established renewable energy source contributing 14.6 TWh of electric power per year [8]. Both wind and geothermal power sources are technologies that already reached satisfactory efficiency; on the other hand, photovoltaics still have room for improvement, the main advantage being the availability of the solar resource and low maintenance. Drawbacks include weather-dependent performance, high initial cost and low efficiency [8]. Therefore, enhancing the performance and lowering the production price of photovoltaic cells are viable ways to advance the transition to green power.

Photovoltaic solar cells convert sunlight into electricity [8]. The cells are generally based on silicon elements, perovskites, organic materials or multi-junction architectures. Each type could be enhanced or made cheaper by incorporating layered transition metal dichalcogenides (TMDs) like, for example, MoS_2 or WS_2 [9, 10, 11]. Single or few layered TMDs exhibit properties unparalleled by their bulk counterparts [12], since they display sizeable and direct band-gaps [9, 12].

Enhancement of a perovskite heterojunction solar cell by using a conductive polymer has been demostrated by using PEDOT:PSS (polystyrene sulfonate) blend with MoS_2 as a hole transport layer. Concretely, the enhancement in power conversion efficiency (PCE) is from 14.69% to 16.47%, accompanied by an increase of the short circuit current and open circuit voltage from 23.874 mA/cm^2 and 0.984 V to 24.035 mA/cm^2 and 0.998 V, respectively [13].

An enhancement in dye sensitised solar cells was shown using a vertically

sensitised MoS_2 substitute for a platinum counter electrode, while MoS_2 was deposited directly onto fluorine-doped tin oxide glass. In this case, the PCE was increased from 7.28 % with Pt to 7.50 % by using an MoS_2 electrode [14].

The examples briefly mentioned above show how transition metal dichalcogenides may improve the efficiency of photovoltaic cells. In this respect, the present work aims to study TMD-based structures by means of ab initio simulations, in order to identify new phases with potential applications in the renewable energy field.

Chapter 2

Theory and computational techniques

The first mandatory step to start the atomistic simulation of our interest is to assess which level of theory is necessary to use for our purposes. Since we want to describe the material structures with atomic detail, two major atomic simulation techniques may be considered, namely molecular dynamics and quantum mechanics. Molecular dynamics technique is built on Newton's classical mechanics which neglects the quantum effects, and every interaction between the atoms is approximated by a set of predetermined potentials (*force field*). On the other hand, quantum mechanical simulations are able to describe the quantum nature of the system, by explicitly describing the electron interactions and how they determine the system properties. Unlike the classical mechanics, the quantum mechanical description does not introduce any ad hoc parameterization of the system; for this reason, this approach is called *ab initio*, that is, without any a priori description. Quantum mechanical simulations enable us to calculate the electronic properties of the system, among them the electronic band gap about the Fermi level, which is the central quantity of interest of the present study. Such band gap is the energy difference between the highest bound state and the lowest conduction state. In other words, it states the lowest energy a photon must have in order to excite an electron to the conduction band (free electron state). In order to evaluate the electronic band gap, the Schrödinger equation for the system of electrons must be solved. Therefore, the level of theory that meets our need is the quantum mechanics and is the one that we choose for the present study.

2.1 The Schrödinger equation

In quantum mechanics the time evolution of the state of a system is described by the Schrödinger equation:

$$i\hbar\frac{\partial\Psi(\boldsymbol{r},t)}{\partial t} = H(\boldsymbol{r},t)\Psi(\boldsymbol{r},t) \tag{2.1}$$

where the solution $\Psi(\boldsymbol{r},t)$ is said to be the *wave function* of the system, and depends on the positions of the particles $\boldsymbol{r}$ and the time t, while H is the Hamiltonian operator, which represents the total energy of the system.

When the Hamiltonian does not depend on the time, it is possible to separate the Schrödinger equation into a time-dependent and a time-independent part. To see this, let us consider a Hamiltonian operator of the form:

$$H = -\frac{\hbar^2}{2m}\Delta + V(\boldsymbol{r}) \tag{2.2}$$

where Δ is the Laplace operator, representing the kinetic energy of the system particles and $V(\boldsymbol{r})$ is the potential representing the interactions between the particles. Let us consider a solution of the form:

$$\Psi(\boldsymbol{r}, t) = \psi(\boldsymbol{r})\theta(t) \tag{2.3}$$

After plugging equation (2.2) and equation (2.3) into equation (2.1) and dividing by $\psi\theta$ we obtain

$$i\hbar\frac{1}{\theta}\frac{d\theta}{dt} = -\frac{\hbar^2}{2m}\frac{1}{\psi}\Delta\psi + V(\boldsymbol{r}) \tag{2.4}$$

Since the left hand side and the right hand side are invariant under any change in $\boldsymbol{r}$ and in t, respectively, equation (2.4) can be split into:

$$i\hbar\frac{d\theta}{dt} = E\theta \tag{2.5}$$

$$-\frac{\hbar^2}{2m}\Delta\psi + V(\boldsymbol{r})\psi = E\psi \tag{2.6}$$

The solution of the time-dependent equation (2.5) is proportional to a complex exponential function. The time-independent equation (2.6) has the form of an eigenvalue-eigenvector equation for the Hamiltonian operator:

$$H\psi(\boldsymbol{r}) = E\psi(\boldsymbol{r}) \tag{2.7}$$

where $\psi(\boldsymbol{r})$ is the time-independent wave function and E is the total energy of the system [15]. By comparing equation (2.4) and equation (2.7), we can appreciate that the latter allows a simpler search for the solution (the time derivative is absent as is the time dependence). It is important to note the Hamiltonian was assumed to be time independent. The assumption constrains the potential V, ensuring its time invariance. In other words, external forces which vary with the time (e.g. time-varying magnetic fields) are not expected to act on the system. When this assumption holds, the equation (2.4) can be separated and the solution simplified so that the eigenvalue-eigenvector equation (2.7) is enough to calculate the wave function $\psi(\boldsymbol{r})$. The resulting wave function allows for a calculation of any physical property that can be observed on the system.

2.2 Born-Oppenheimer approximation

The only case where equation (2.7) can be solved analytically is the hydrogen atom without the spin-orbit interaction; the wave function of any other system has to be evaluated numerically [15].

Obtaining a numerical solution of the Schrödinger equation is not as straightforward as it may seem, because the process implies the use of algorithms and approximate expressions, which produce results within a limited accuracy. Besides the many technical aspects of the modelling process such as number truncation, numerical noise or the approximation of integrals or derivatives, let us consider first those approximations related to the physical properties of the system. Such approximations neglect or approximate a complicated part of the physical description. Specifically, equation (2.7) is an equation for the system as a whole. Therefore, equation (2.7) solves the wave functions of nuclei and electrons at the same time. Separating equation (2.7) into an equation for the nuclei and for the electrons would help us find the solution. Since the mass of a nucleus is significantly larger than the mass of an electron, it is possible to assume that the motion of the nuclei is much slower that that of the electrons. In other words, electrons can react almost instantly to any change of position of the nuclei, and the latter can be considered still. Therefore, a time invariant potential created by the nuclei clamped to their position is used to solve the electronic part of the Schrödinger equation. This approach is called the *Born-Oppenheimer approximation* and allows the separation of equation (2.7) into an electronic and a nuclear equation. However, neglecting the motion of nuclei causes an inaccuracy for systems not in the ground state; this inaccuracy is increasing with increasing energy of the nuclei.

The expression of the Born-Oppenheimer approximation starts with a Hamiltonian in form:

$$H = T_e + T_N + V = -\frac{\hbar^2}{2m_e}\Delta - \sum_{j=1}^{n}\frac{\hbar^2}{2M_j}\frac{\partial^2}{\partial \boldsymbol{R}_j^2} + V(\boldsymbol{r}, \boldsymbol{R}) \tag{2.8}$$

where T_e and T_N are the kinetic energies of the electrons and the nuclei, respectively, and V is the potential; $\boldsymbol{R}$ is a $3n$-dimensional vector formed by the coordinates of the n atoms forming the system, while $\boldsymbol{R}_j$ refers to the triplet relative to the j-th atom. Within our assumption, the nuclear positions $\boldsymbol{R}$ act as parameters for the electronic Schrödinger equation:

$$H\Psi(\boldsymbol{r}, \boldsymbol{R}) = E\Psi(\boldsymbol{r}, \boldsymbol{R}) \tag{2.9}$$

where $\boldsymbol{r}$ is the multidimensional vector for the electron positions. We consider a tentative solution Ψ in the form

$$\Psi(\boldsymbol{r}, \boldsymbol{R}) = \psi(\boldsymbol{r}, \boldsymbol{R})\chi(\boldsymbol{R}) \tag{2.10}$$

where $\psi(\boldsymbol{r}, \boldsymbol{R})$ is the electronic wave function and $\chi(\boldsymbol{R})$ is the wave function for the nuclei. Plugging equation (2.10) into equation (2.9) yields

$$H\psi\chi = \chi T_e\psi + \psi T_N\chi + V\psi\chi + W = E\psi\chi \tag{2.11}$$

where W is the mixing term

$$W = -\sum_{j=1}^{n}\frac{\hbar^2}{2M_j}\left(2\frac{\partial\psi}{\partial \boldsymbol{R}_j}\frac{\partial\chi}{\partial \boldsymbol{R}_j} + \frac{\partial^2\psi}{\partial \boldsymbol{R}_j^2}\chi\right) \tag{2.12}$$

which is usually neglected because the mass of the nuclei M_j is large and appears at the denominator of each term of the sum. However, when the kinetic energy of the nuclei is large, W cannot be neglected. Following this approximation, equation (2.11) can be separated into an equation for the nuclei and for the electrons respectively:

$$T_N\chi + E_e\chi = E\chi \tag{2.13}$$

$$H_e\psi = T_e\psi + V\psi = E_e(\boldsymbol{R})\psi. \tag{2.14}$$

2.3 Self Consistent Field

The result of the Born-Oppenheimer approximation offers a simplification of the Schrödinger equation of a system. Even though the number of variables has been decreased (the nuclear positions $\boldsymbol{R}$ are parameters after applying the Born-Oppenheimer approximation), the equation (2.14) is still complicated enough that further approximations to solve the electronic wave function are necessary. *The Hartree-Fock method* [15] introduces an approximation of the electron-electron interaction, which assumes that each electron is moving in a spherical average potential of all the other electrons. Furthermore, the solution is found by an iterative scheme which is stopped when specific criteria are satisfied.

The iterations proceed according to the following steps:

1. An initial tentative electronic wave function is assumed as a function of hydrogenic orbitals
2. The spherical average potential is constructed
3. The wave function solution of the equation is evaluated
4. The resulting wave function for all the electrons is used as a new input in item 2, unless the convergence criteria have been satisfied; in the latter case, the iterations are stopped and the resulting wave function is the solution of the Schrödinger equation.

A possible convergence criterion can be specified as a maximal difference of a chosen quantity between two subsequent iterations. The quantity governing the termination of the procedure can be the total energy of the system, the maximum force on the atoms or others. When the convergence criterion is satisfied, then the wave function is said to be *self-consistent*, as it is the solution of the *self-consistent field* iterative scheme just outlined.

The steps listed above give a qualitative description of the procedure. Let us take a closer look at each of them. In item 1 in the list, the Hamiltonian of the system is approximated by a hydrogenic *core Hamiltonian* for each electron:

$$H = \sum_{i=1}^{n} h_i \quad | \quad h_i = \frac{\hbar^2}{2m_e}\Delta - \frac{Ze^2}{4\pi\epsilon_0 \boldsymbol{r}_i} \tag{2.15}$$

where Δ is the Laplacian, $\boldsymbol{r}_i$ is the distance of the electron i from the nucleus and Z is the atomic number of the nucleus. This allows for a separation of the Schrödinger equation into one-electron equations of the form:

$$h_i \psi_a^o(i) = E_a^o \psi_a^o(i) \tag{2.16}$$

The solution of each equation yields a one-electron wave function $\psi_a^o(i)$ and a corresponding energy E_a^o.

The second step (item 2) corresponds to the sum over all the orbitals u:

$$\sum_u [J_u(i) - K_u(i)] \tag{2.17}$$

where $J_u(i)$ is the *Coulomb operator* and $K_u(i)$ is the *exchange operator* for the i-th electron, respectively. The former describes the electron-electron repulsion while the latter describes the change in energy due to the spin correlation. Both are calculated as an interaction between two electrons and evaluated by integration. Equation (2.17) is part of the definition of the *Fock operator*:

$$f_i = h_i + \sum_u [J_u(i) - K_u(i)]. \tag{2.18}$$

The Item 3 is the evaluation of the *Hartree-Fock equations* which have the form

$$f_i \phi_a(i) = \epsilon_a \phi_a(i) \tag{2.19}$$

where f_i is the *Fock operator*, $\phi_a(i)$ is the spinorbital (a modified type of one-electron wave function $\psi_a^o(i)$) and ϵ_a is the energy relative to a given spinorbital ϕ_a. For each electron, the corresponding equation (2.19) is solved, and produces new spinorbitals which are substituted as an input of the next iteration - item 4.

The solution of the above equation proceeds from the basis expansion:

$$\phi_i = \sum_{j=1}^{M} c_{ji} \Theta_j \tag{2.20}$$

where c_{ji} are the coefficients of the expansion and Θ_j are the basis functions (Slater-type orbitals or Gaussian-type orbitals) [15]. This expansion is then plugged into the equation (2.19) giving the *Roothaan equations*:

$$\mathbb{F}\boldsymbol{c} = \mathbb{S}\boldsymbol{c}\boldsymbol{\epsilon} \tag{2.21}$$

where $\mathbb{F}$ is the *Fock matrix*, $\mathbb{S}$ is the *overlap matrix*, $\boldsymbol{c}$ is the $M \times M$ matrix of the coefficients c_{ji} (M is the number of basis functions in equation (2.20)) and $\boldsymbol{\epsilon}$ is a diagonal matrix of the orbital energies. By using the properties of the matrix equations, equation (2.21) has non-trivial solution only when

$$\det |\mathbb{F} - \boldsymbol{\epsilon}\mathbb{S}| = 0. \tag{2.22}$$

However, it is not possible to solve the equation directly, because the elements of the matrix $\mathbb{F}$ depend on the wave functions ϕ_a which we have to obtain in the first place. This circular dependence is the reason for the iterative approach used to solve the electronic Schrödinger equation.

2.4 Density functional theory

The Hartree-Fock method struggles with systems with a large basis. The struggle lies in the calculation of the exchange and Coulomb operators. The interaction among whole set of orbitals is decomposed into two-electron interactions and evaluated as two integrals, one for the Coulomb and one for the exchange operator. The resulting calculation time is proportional to the fourth power of the number of basis functions. Moreover, the major drawback of the Hartee-Fock approach is the lack of the correlation energy in the Hamiltonian [16]. The Density functional theory (DFT) [17, 18] solves both issues: it reduces the computational load by considering the *electron probability density* as the central quantity to be evaluated and includes the correlation effects in the expression for the total energy of the system. The electron probability density $\rho(\boldsymbol{r})$ describes the ground state electron density at a given point $\boldsymbol{r}$ in the space; it is defined as

$$\rho(\boldsymbol{r}) = \sum_{i=1}^{n} |\psi_i(\boldsymbol{r})|^2 \tag{2.23}$$

where the sum runs over all the occupied orbitals $\psi_i(\boldsymbol{r})$, the latter named *Kohn-Sham orbitals*. Note that, in equation (2.23), the number of variables is reduced from $3n$ to 3 for a system of n electrons. The Kohn-Sham orbitals are obtained by solving the Kohn-Sham equations, which are derived by the application of the variational principle on the equation for the total energy [15]. The total energy of a system is written as a functional of the electron probability density $\rho(\boldsymbol{r})$:

$$E[\rho] = T_{el}[\rho] + I_{n-el}[\rho] + I_{Coul}[\rho] + E_{XC}[\rho] \tag{2.24}$$

where T_{el} is the kinetic energy of all the electrons, I_{n-el} is the interaction between nuclei and electrons, I_{Coul} is the coulombic interaction and E_{XC} is the *exchange-correlation energy*.

To calculate the density $\rho(\boldsymbol{r})$, the Kohn-Sham orbitals are needed.
This is achieved by the following iterative approach

1. An initial guess for the density ρ is provided
2. An Approximate form for E_{XC} is chosen
3. The Kohn-Sham equations are solved to obtain the Kohn-Sham orbitals
4. The Kohn-Sham orbitals are used to create an improved guess for the density ρ

The calculation continues until the convergence is reached by satisfying selected criteria as for the Hartree-Fock method (section 2.3).

Within the DFT framework, several approximations exist for the explicit form of the Hamiltonian. In the *local density approximation* (LDA), the electron distribution is estimated by considering a homogeneous electron

gas of constant density. Additionally, a uniform, continuous, positive charge distributed over the whole space is considered in order to ensure the electroneutrality. The exchange-correlation functional E_{XC} is then calculated by assuming that the electrons interact with each other as if they were in a homogeneous electron gas. Although it seems a rough approximation of the real interaction, the LDA can be used to calculate structural properties with satisfactory accuracy in specific systems [19]. However, the accuracy decreases with decreasing homogeneity of the electron density; in this case, the *generalised gradient approximation* (GGA) is used [20, 21, 22, 23]. The GGA makes use of the gradient of the density which accounts for significant variations of the electron distribution across the system.

2.5 Direct and reciprocal lattice

A crystalline solid is a 3D periodic structure of repeating groups of atoms, the latter referred to as the *basis*. This type of structure is but an idealization of the corresponding real structure.

2.5.1 Direct lattice

The mathematical description of a crystal is provided by the concept of *direct lattice*. The direct lattice is defined by three linearly independent vectors $\boldsymbol{a}_{1,2,3}$. Two equivalent positions $\boldsymbol{r}$ and $\boldsymbol{r'}$ are connected by a linear combination of vectors $\boldsymbol{a}_{1,2,3}$:

$$\boldsymbol{r'} = \boldsymbol{r} + u_1\boldsymbol{a}_1 + u_2\boldsymbol{a}_2 + u_3\boldsymbol{a}_3 = \boldsymbol{r} + \boldsymbol{T} \tag{2.25}$$

where $u_{1,2,3}$ are integers defining the *translation vector* $\boldsymbol{T}$. The points in the space which satisfy equation (2.25) are called *lattice points*. To illustrate the geometrical significance of equation (2.25), let's imagine a photographer with the size of an atom. If he takes one 360° photograph standing exactly on the point $\boldsymbol{r}$ and one on the point $\boldsymbol{r'}$, then the two photos will be identical.

The vectors $\boldsymbol{a}_{1,2,3}$, which are a basis of the 3D-space, define the *crystal axes*, and the parallelepiped formed by the basis vectors is called the *unit cell*. If the unit cell has a minimal volume, then it is called *primitive cell*; it is not possible to find a smaller unit that reproduces the whole structure. The primitive cell contains exactly one lattice point and its choice is not unique [24].

Equation (2.25) defines a translation vector, which translates the lattice onto itself, creating *translational symmetries*. All the possible three-dimensional lattice translational symmetries define 14 crystallographyc families called the *Bravais lattices*. Associating a group of atoms to each lattice point creates more symmetry operations that can transform the lattice into itself, such symmetries including rotations or mirror planes among others [24]. The set of such symmetry operations, excluding the translational symmetries, is called the *lattice point group*. By combining the Bravais lattices with the point groups, a full description of the lattice symmetry is obtained, named *space group*.

2.5.2 Reciprocal lattice

The reciprocal lattice provides a convenient way to describe the physical properties of a crystal. Physical properties are represented by functions, which in the case of a crystal are periodic; in this conditions, the use of the Fourier analysis is the natural way to exploit such periodicity. The Fourier analysis transforms a function into a weighted sum of complex exponential functions representing plane waves. Each plane wave is characterised by a wave vector, which can be expressed as a linear combination of $\boldsymbol{b}_{1,2,3}$ basis vectors defined in this way:

$$\boldsymbol{b}_1 = 2\pi \cdot \frac{\boldsymbol{a}_2 \times \boldsymbol{a}_3}{\boldsymbol{a}_1 \cdot \boldsymbol{a}_2 \times \boldsymbol{a}_3}; \quad \boldsymbol{b}_2 = 2\pi \cdot \frac{\boldsymbol{a}_3 \times \boldsymbol{a}_1}{\boldsymbol{a}_1 \cdot \boldsymbol{a}_2 \times \boldsymbol{a}_3}; \quad \boldsymbol{b}_3 = 2\pi \cdot \frac{\boldsymbol{a}_1 \times \boldsymbol{a}_2}{\boldsymbol{a}_1 \cdot \boldsymbol{a}_2 \times \boldsymbol{a}_3} \tag{2.26}$$

where $\boldsymbol{a}_{1,2,3}$ are the crystal lattice vectors. The $\boldsymbol{b}_{1,2,3}$ vectors define the *reciprocal lattice*, which is the Fourier transform image of the direct lattice.

The primitive unit cell in the reciprocal space, corresponding to the transformed primitive cell of the direct lattice, is called *Brillouin zone*. The Brillouin zone of the systems considered in this study is reported in figure 2.1.

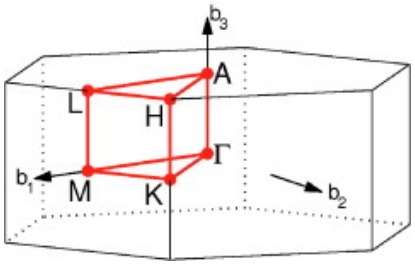

Figure 2.1: The Brillouin zone of the hexagonal lattice. The capital letters label the high symmetry points. Adapted from Ref. [1].

2.6 The Bloch functions

The periodic structure of a crystal, owning a periodic atomic potential, intuitively suggests that the electronic wave function is also periodic. This hypothesis is proved by the Bloch's theorem, stating the form of the electronic wave function $\psi_{\boldsymbol{k}}(\boldsymbol{r})$:

$$\psi_{\boldsymbol{k}}(\boldsymbol{r}) = u_{\boldsymbol{k}}(\boldsymbol{r}) \cdot e^{i\boldsymbol{k}\cdot\boldsymbol{r}} \tag{2.27}$$

where the electronic wave function is labeled by a wave-vector $\boldsymbol{k}$, $e^{i\boldsymbol{k}\cdot\boldsymbol{r}}$ represents a plane wave and $u_{\boldsymbol{k}}(\boldsymbol{r})$ is a periodic function with the periodicity of the crystal: $u_{\boldsymbol{k}}(\boldsymbol{r}) = u_{\boldsymbol{k}}(\boldsymbol{r} + \boldsymbol{T})$.

The decomposition of the electronic wave function, solution of the Schrödinger equation, by means of the Bloch's functions of the form equation (2.27) is a convenient choice. Indeed, multiple energy values correspond to each wave vector $\boldsymbol{k}$ as a result of the eigenvalue-eigenvector equation (2.14). The set of

all the possible energy values corresponding to a set of chosen wave vectors is referred as the *electronic band structure*.

Similarly, there can be several k-points corresponding to a single energy value. A histogram mapping the count of all k-points corresponding to a single energy value is called *density of states*. The k-points corresponding to energy values are obtained in the same way as for the electronic band structure. However, the sampling of the Brillouin zone is homogeneous in the whole volume in contrast to the set of k-points chosen for the electronic band structure.

The inspection of all the energy values satisfying equation (2.14) provides information about the energy gaps, which are the energy ranges that are not accessible to the electrons in the system. In fact, the electrons are described by states represented by linear combinations of Bloch's functions: no states are available to the energy values forming the energy gaps of the system. The energy gap between the last occupied state and the first unoccupied state is the most relevant gap as it determines the conductivity and most of the optical properties [24]. For this reason, such gap is the subject of the present study.

2.7 Geometry optimisation

The theoretical framework that we presented above is the basis for the construction of a model of a quantum system; in parallel to such framework, other assumptions must be done in order to build a reliable representation of the real compound. In general, the geometry of the systems can be faithfully modeled by considering the atom configuration which realizes the minimum of the system energy. Therefore, finding such configuration is an important part of the atomic simulation. The nuclei contribute to a major part of the potential energy of the whole system, and manipulating their arrangement may be used to minimize the total energy.

The term *geometry optimisation* refers to a procedure that obtains the minimum of the potential by varying the position of the nuclei. Firstly, the Born-Oppenheimer approximation separates the wave function of the whole system into electronic and nuclear parts. Then the electronic part is solved by the self consistent field cycle, so that the total electronic energy is obtained. Now the positions of the nuclei have to be adjusted in order to lower the energy. The atomic coordinates are modified along the direction that realizes the opposite of the energy potential gradient with respect to the nuclear positions; in this way, the structure evolves towards the minimum of the potential energy. The forces acting on the atoms are then calculated by means of the Hellmann-Feynmann theorem [25]. The whole procedure is repeated until the forces are minimized below a certain tolerance set at the beginning of the optimisation cycles.

2.8 Used software

The present study is conducted by using the quantum mechanical ab initio package ABINIT [26, 27, 28, 29]. ABINIT is a free simulation software which allows to find the solution of the Schrödinger equation and obtain the related quantities such as the total energy, the optimised geometry, the charge density and electronic structure of the considered system. In ABINIT, the Schrödinger equation is solved in the framework of the Density Functional Theory by means of a plane-wave basis decomposition.

Chapter 3

Systems derived from Transition Metal Dichalcogenides

The transition metal dichalcogenides (TMDs) are compounds with general formula MX_2, where M is a transition metal and X is a chalcogen atom [12]; in this study, we select M = Mo, W and X = S, Se Te. TMDs are crystalline structures formed by layers of atoms coupled by covalent bonds [9]; each layer is formed by a transition metal cation coordinating 6 chalcogen anions in a prismatic fashion. The layers are held together by Van der Waals forces, which are weak enough to reduce the bulk material into few- or single-layer thin films [30, 31]. A schematic example of the TMD atom geometry is reported in Figure 3.1.

The starting geometry for the simulations of the pristine compounds is the experimentally determined unit cell of the corresponding bulk material [32, 33, 34, 35, 36, 37]. From the bulk structure, two and three layers have been isolated by adding a vacuum slab of about 50Å; this procedure ensures us that no interactions are present between image replicas along the *c*-axis in our setting. In this way, we build the two and three layer MX_2 models for the pristine systems which we name 2L-MX and 3L-MX, where M and X specify the kind of cation and anion, respectively.

To simulate doped systems, we consider $2 \times 2 \times 1$ supercells of the pristine structure. In the 2L-MoX systems, we substitute one Mo atom with one W atom, thus obtaining what we name the W:2L-MoX models; by doing the analogous substitution in the 2L-WX systems, we obtain the Mo:2L-WX models. We will refer to both as Z:2L-MX, where Z is the substituting cation and Z$\neq$M. In the 3L-MX models, the substitution is performed in one of the two external layers or in the middle layer, thus building the Z:3L-L1-MX and the Z:3L-L2-MX systems, respectively; here Z has the same meaning as for the Z:2L-MX models. A schematic representation of the geometries of the doped compounds is reported in Figure 3.2.

An initial benchmark is performed on the pristine systems in order to determine the optimal parameters for the simulations. According to the benchmark, we choose a $11 \times 11 \times 1$ Monkhorst-Pack [38] grid division for the integration in the Brillouin zone, and select 750 eV and 850 eV as plane wave and PAW energy cutoff, respectively. The Perdew-Burke-Ernzerhof GGA functional [21] is used to describe the interatomic interactions, while the

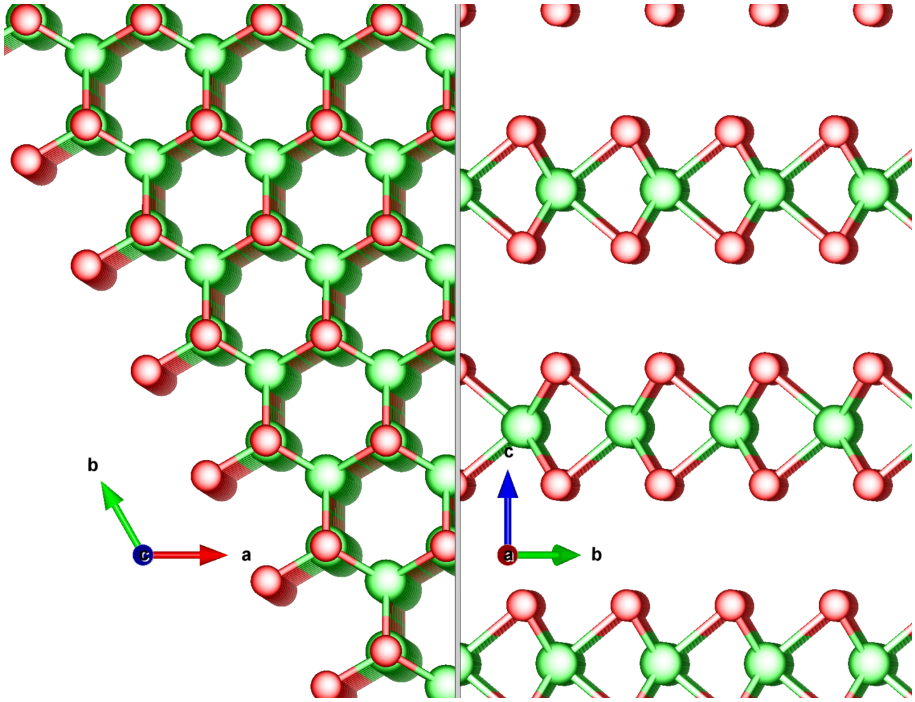

Figure 3.1: Bulk geometry of a generic TMD. The green and red spheres represent the M cations and the X anions, respectively. Left panel: view from the "top" showing the typical hexagonal arrangement of the atoms within each layer (c-axis coming out of the plane of the page). Right panel: view from the "side" showing the characteristic layer structure (a-axis coming out of the plane of the page).

Van der Waals forces are parameterized with the vdf-DFT-D3(BJ) Grimme correction [39] based on the Becke-Jonhson method [40], with a tolerance of 10^{-10} to include the 3-body term. The SCF energy minimization is considered converged when the energy difference between two subsequent cycles is less than 10^{-10} eV; the geometric optimisation is stopped when the largest force component is smaller than 5×10^{-8} eV/Å.

3.1 Geometry analysis

The pristine bulk structures own the symmetries of the space group $P6_3/mmc$ (194); unsurprisingly, it is the structure with the highest number of symmetry operations among all the considered systems. In fact, the first effect of truncating the periodicity of the bulk geometry is the reduction of the symmetries. The 2L structures show the symmetries of the $P\bar{3}m1$ (164) space group; a similar change can be observed for the transition from bulk to the 3L models where the symmetry is reduced to $P\bar{6}m2$ (187). The cation substitution in the 2L systems removes the inversion center and further lowers the symmetries down to the $P3m1$ (156) space group. The doping in the Z:3L-L1 cases has the effect to lift the inversion symmetry as in the case of the

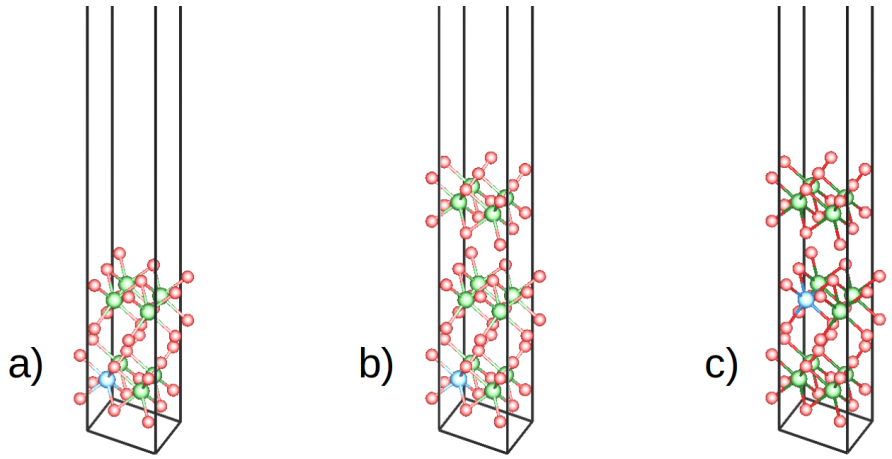

Figure 3.2: Schematic model of the (a) Z:2L-MX, (b) Z:3L-L1-MX and (c) 3L-L2-MX systems. The green, red and blue spheres indicate the position of the M cation, the X anion and the Z dopant, respectively. The periodicity of the bulk is truncated by adding a vacuum slab parallel to the layer plane. The solid black lines indicate the unit cell, trimmed from the top part for the sake of simplicity of the figure representation.

System	Space Group
bulk	$P6_3/mmc$ (194)
2L	$P\bar{3}m1$ (164)
Z:2L	$P3m1$ (156)
3L	$P\bar{6}m2$ (187)
Z:3L-L1	$P3m1$ (156)
Z:3L-L2	$P\bar{6}m2$ (187)

Table 3.1: Space groups of the model systems; the Hermann-Mauguin notation is used and the corresponding space group number is reported in parentheses [2].

Z:2L systems, leading to the same space group $P3m1$ (156). However, in the Z:3L-L2 systems, the doping in the middle layer preserves the inversion center and leaves the symmetries of the undoped 3L reference structure unaltered. The space groups of all the model systems are collected in Table 3.1; the complete structure definition of each optimised geometry is reported in the Appendix chapter.

Now we take a close look at the interatomic distances, in order to quantify the detail of the atom geometry (Figure 3.3). Irrespective of the number of layers and the kind of doping, the M-X distances as found in the pristine structure remain almost unaltered after the insertion of the dopant atom; similarly, the Z-X distances are nearly identical to the M-X distances before the substitution. In both cases, the overall variation is of about 0.01Å. The type of anion present in the compound determines the magnitude of the M-X and the Z-X distances. For a given anion X, the cation M has far lesser impact on the M-X distances than the anion. This is apparent from the

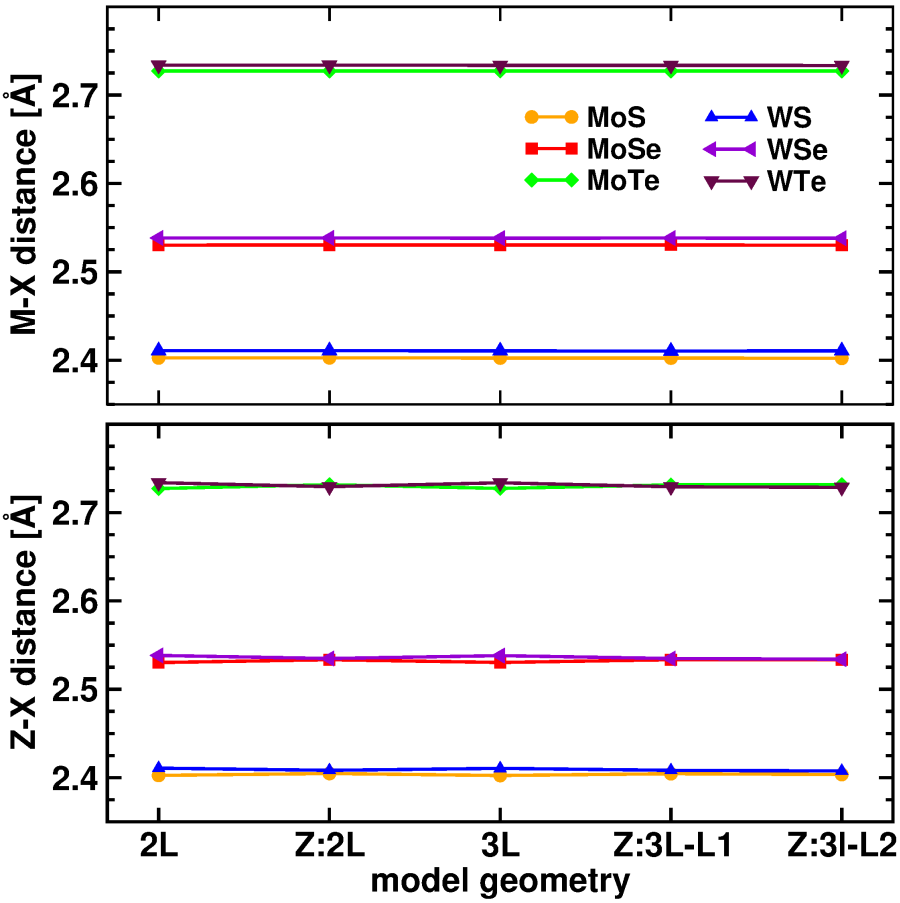

Figure 3.3: M-X and Z-X distances plotted as a function of the kind of system. The overall geometric arrangement does not have a significant effect, as well as the kind of cation. The magnitude of the distances is mainly determined by the atomic type of the anion.

distance distribution reported in Figure 3.3: the values form three distinct groups characterized by the kind of anion.

3.2 Electronic analysis

We begin the electronic analysis by examining the variation of the band gap size at varying geometry (Figure 3.4). We first observe that, irrespective of the geometry and at fixed cation, the band gap decreases as S>Se>Te; this indicates that the atomic type of the anion has the major influence in the band gap ordering. Another factor which mainly determines the size of the band gap is the number of layer. In fact, we find that, irrespective of the compound and the kind of dopant, the value of the gap found in the 2L systems decreases upon adding an extra layer.

In general, in the 2L systems the band gap increases after the insertion of the dopant; an exception is found for the compounds containing tellurium,

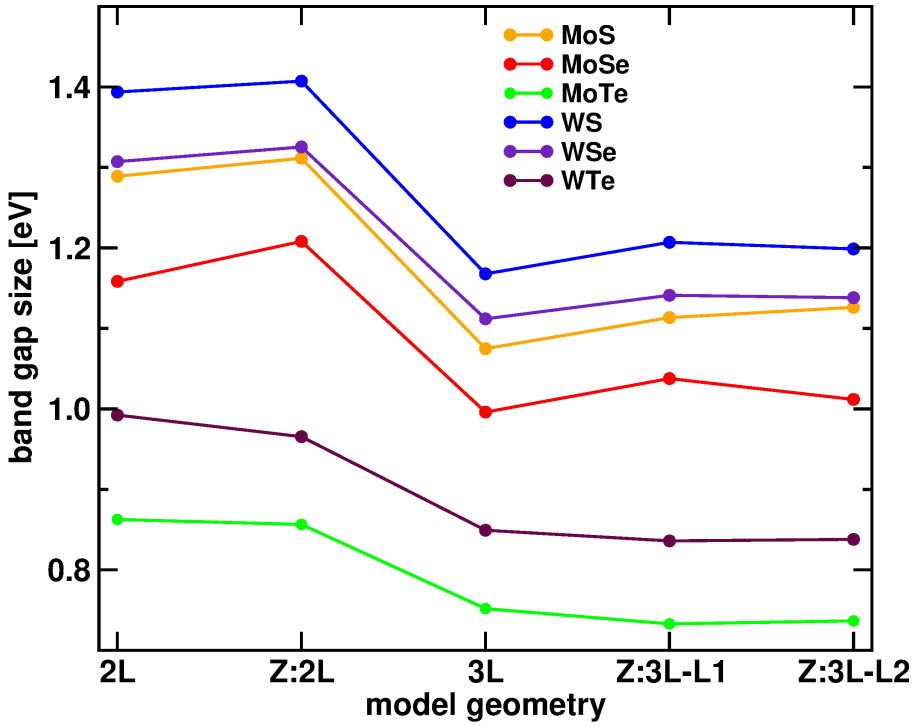

Figure 3.4: Band gap size as a function of the model geometry. The main factors determining the gap values are the number of layers and the kind of anion forming the structure.

whereas the change in the gap value is small. A similar behaviour is observed for most of the 3L systems. The doping of one of the external layers (3L→Z:3L-L1) widens the band gap; similar behaviour is found when the substitution is performed in the middle layer (3L→Z:3L-L2). Interestingly, all the 3L systems containing tellurium are not significantly affected by the doping — the change in the gap values is negligible. Therefore, we are inclined to think that the Te anion screens the effect of the dopant on the band gap size in TMD heterostructures. In order to gain more insight on the observed trends, we need to consider the detail of the electronic structure. With this aim, we analyse the atom-projected density of states in the energy range $[-2, 3]$ eV encompassing the electronic band gap about the Fermi level (figures 3.5 and 3.6).

We first observe that all the systems, irrespective of the chemical composition and the number of layer, share common features. The projected-DOS of the dopant atom and the substituted one are very similar; this suggests that the Mo and W cations show similar bonding properties and can be used as reciprocal substituents without altering the electronic distribution in a substantial way. Moreover, both cations and anions contribute in the same amount to the formation of the top of the valence band. On the contrary, the bottom of the conduction band shows characteristics peculiar to the system. In the 2L-MX and 3L-MX systems, the M ion has the greatest contribution

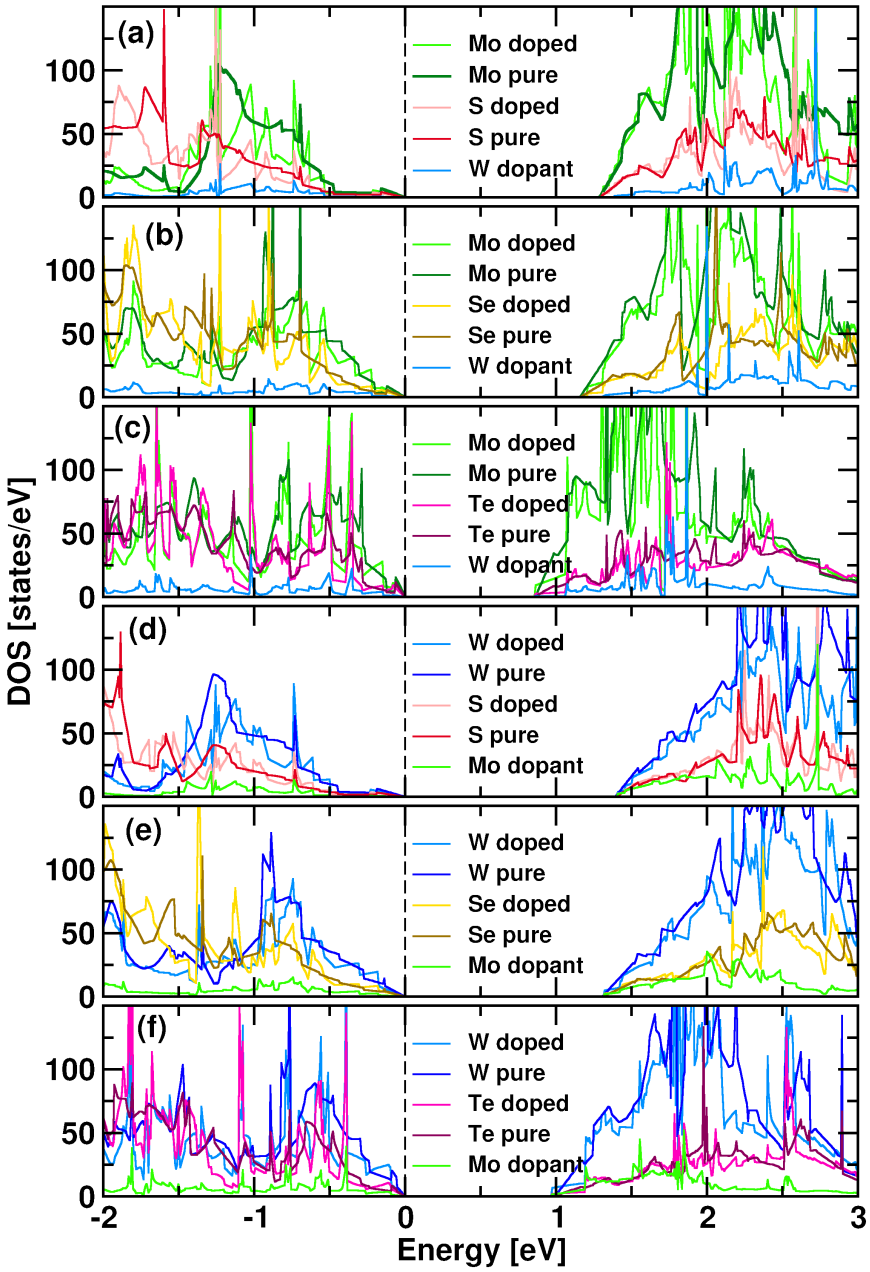

Figure 3.5: Atom-projected density of states of the 2L systems: (a) 2L-MoS and W:2L-MoS, (b) 2L-MoSe and W:2L-MoSe, (c) 2L-MoTe and W:2L-MoTe, (d) 2L-WS and Mo:2L-WS, (e) 2L-WSe and Mo:2L-WSe, (f) 2L-WTe, and Mo:2L-WTe. The DOSs of the doped structures have been normalized by the number of supercells (4). The labels "pure" and "doped" indicate if the data is referring to the ion in the pure or in the doped structure, respectively, while the label "dopant" indicates the atomic type of the Z substituting atom. The Fermi level has been set to 0 eV and is indicated by a vertical dashed line.

to the formation of the energy levels when compared with the X-projected levels; this suggests that the cation plays a key role in the electronic transition covering the band gap in the pristine compounds. In the W-doped systems, the main contribution is due to the native cation (i.e., Mo), while in the Mo-doped compounds both cations produce comparable density of states; this may indicate that, for low concentration of W dopant in Mo-based systems, the substitution does not alter the character of the electronic transition in a significant way.

We now want to have a closer look to the bottom of the valence band, in order to understand the role of the dopant in the determination of the band gap (figures 3.7 and 3.8). In all the systems not containing the Te anion, the hybridization imposed by the dopant determines the contraction of the bottom of the valence band toward levels which are higher in energy than what is found in the corresponding undoped structure. On the countrary, the Te anion participates to such hybridization in such a way to contain the band contraction, leaving the band gap almost unaltered.

In the final part of the analysis, the electronic band dispersion is calculated for each of the studied systems. Surprisingly, the value of the band gap is slightly smaller for some systems than the values obtained from the DOS analysis. This is unusual because the mesh used to sample the electronic states available in the system (i.e., the DOS) is much denser than that one used to sample the electronic band structure along a specific piece-wise linear k-path connecting high-symmetry points. In the present case, the technical choices aimed to improve the performance of the DOS calculations, and related to the symmetries of the studied systems, produced a k-mesh not containing some of the k-points included instead in the band structure calculation. However, the difference between the band gap values found in the two cases is small and does not affect our conclusions. For this reason, the calculated band dispersions are not reported.

3.3 Discussion

Our results show that the structure type has the largest impact on the size of the band gap, specifically, the number of layers. In fact, by increasing the number of layers from 2 to 3, the band gap decreases in an amount $\gtrsim 1.2$ eV. The other structural features, e.g. the interatomic distances or the lattice parameters, do not vary in a significant way by changing the number of layers or after cation substitution; no correlation is then expected between them and the value of the band gap of the corresponding system.

The doping results in fine tuning of the width of the gap. In all the compounds, after cation substitution, the change observed in the gap size ranges from 0.114 to 0.50 eV. A further degree of freedom is added in the 3L systems: in that case, the position of the dopant can be chosen to be in one of the external layers or in the middle one. The position of the dopant in the 3L case determines in general the variation of the band gap within ~ 0.02 eV, and it can be used as a further "knob" to tune the band gap in a more

precise way. However, the presence of the Te anion seems to mitigate the gap size variations induced by the doping or by the dopant position.

Hitherto, only a general overview of the monitored parameters has been presented. Clearly, a more detailed investigation is needed to fully understand how the dopant and its position determine the final band gap value. An analysis of the subtleties of the charge density determined by the dopant (i.e., orbital polarization) could be preformed. Additionally, the character of the Z-X covalent bond and the surrounding M-X bonds should be examined; the covalent character of the latter is expected to be different than the one found in the pristine compound, especially in the neighbourhood of the dopant site. Finally, as an extension of the present work, the consideration of different dopant concentrations will complete the insights about the role of the dopant in the determination of the band gap in heterostructured TMD-based compounds.

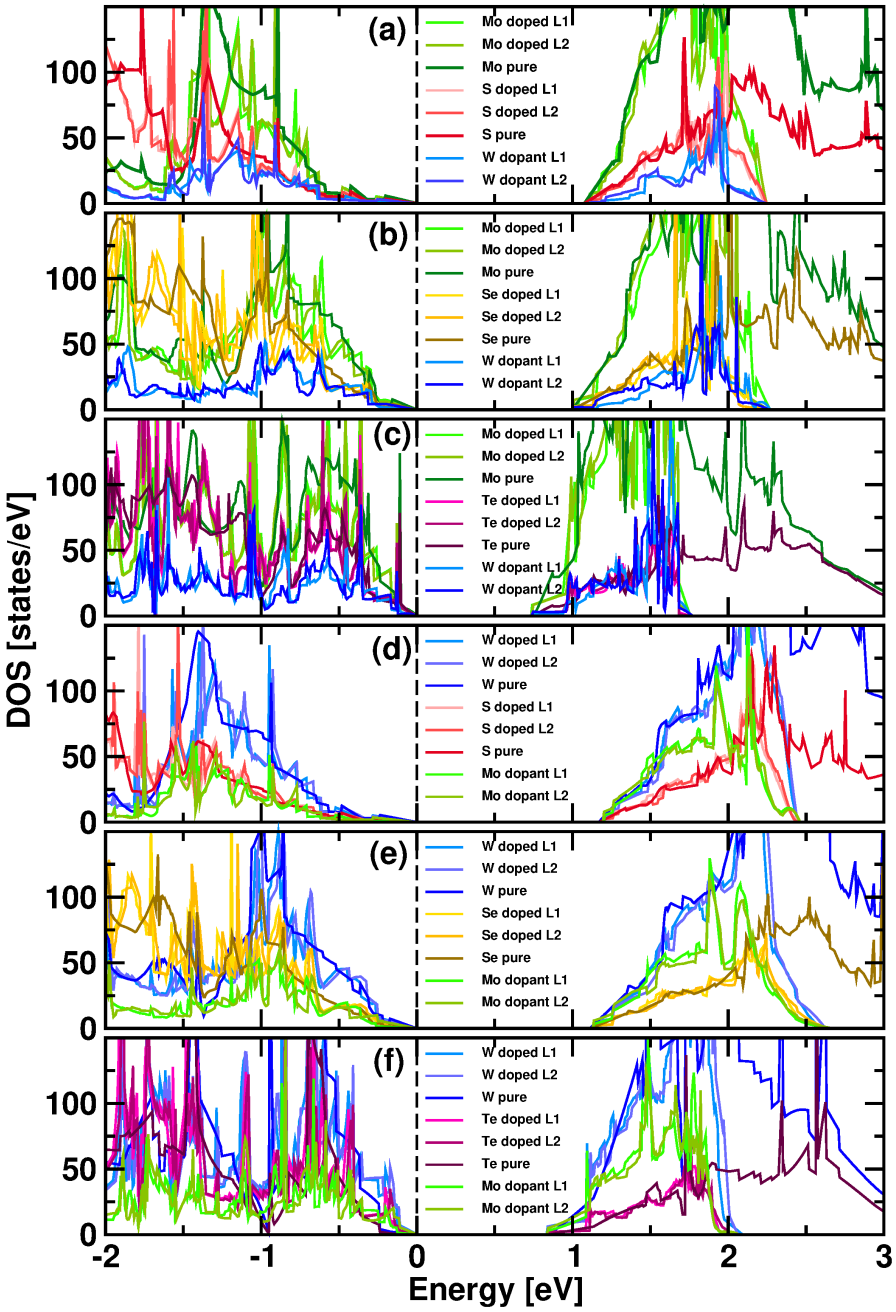

Figure 3.6: Atom-projected density of states of the 3L systems: (a) 3L-MoS, W:3L-L1-MoS and W:3L-L2-MoS (b) 3L-MoSe, W:3L-L1-MoSe and W:3L-L2-MoSe, (c) 3L-MoTe, W:3L-L1-MoTe and W:3L-L2-MoTe, (d) 3L-WS, Mo:3L-L1-WS and Mo:3L-L2-WS, (e) 3L-WSe, Mo:3L-L1-WSe and Mo:3L-L2-WSe, (f) 3L-WTe, Mo:3L-L1-WTe Mo:3L-L2-WTe. The DOSs of the doped structures have been normalized by the number of supercells (4). The labels "pure" and "doped" indicate if the data is referred to the ion in the pure or in the doped structure, respectively, while the label "dopant" indicates the Z substituting atom. The Fermi level has been set to 0 eV and is indicated by a vertical dashed line.

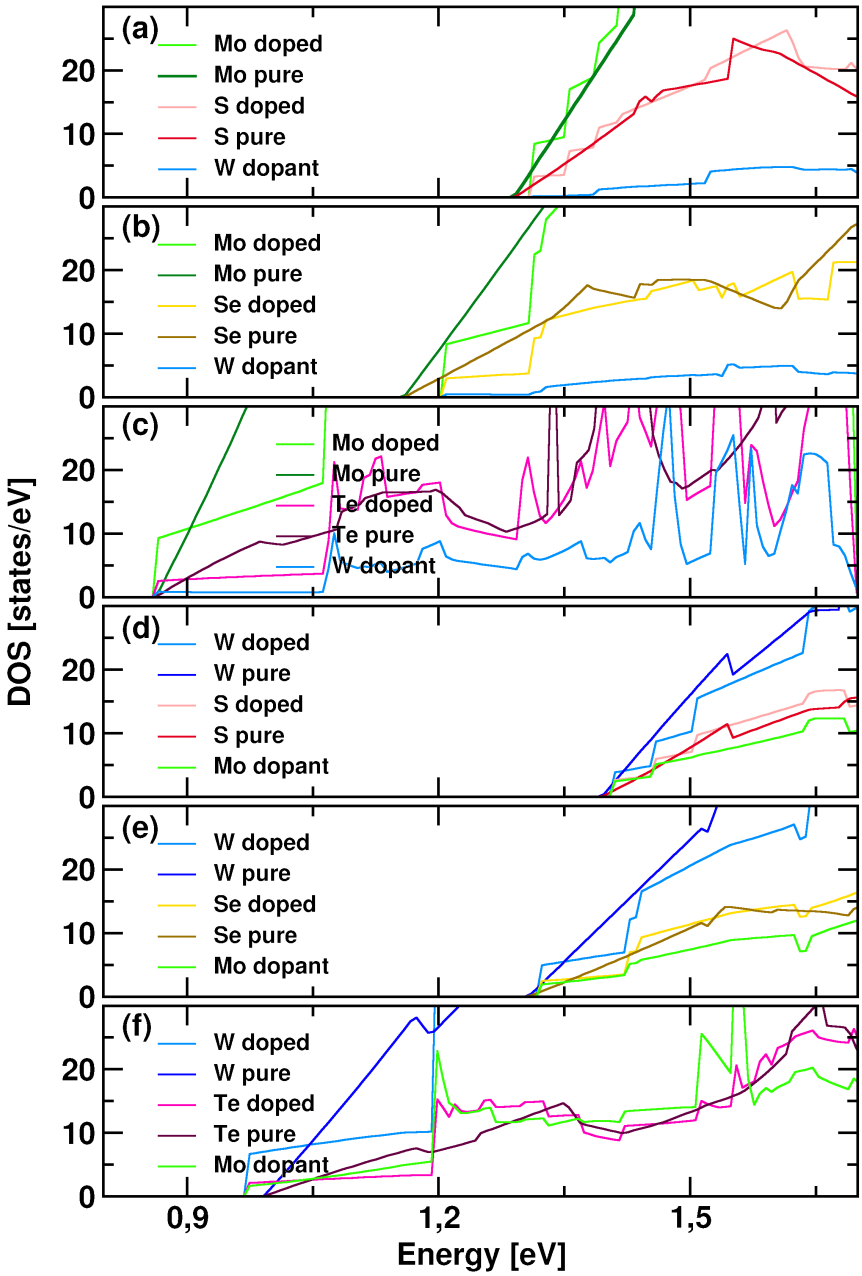

Figure 3.7: Detail of the top of the valence band of the corresponding projected DOS reported in Figure 3.5.

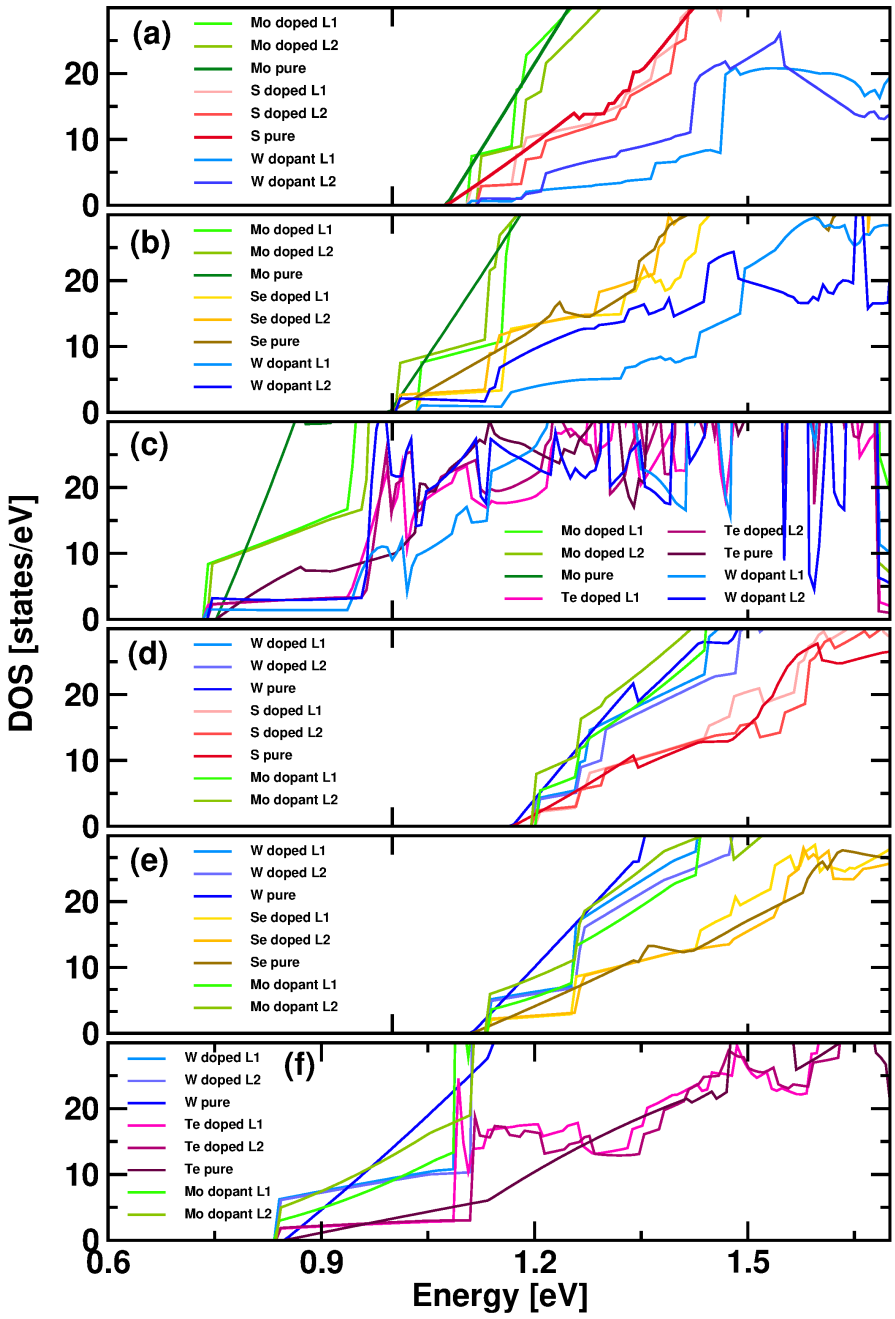

Figure 3.8: Detail of the top of the valence band of the corresponding projected DOS reported in Figure 3.6.

Chapter 4

Conclusions

The influence of doping on the band gap size of selected layered transition metal dichalcogenides has been studied and presented. The study was conducted by using ab initio methods. Such choice allowed us to inspect the quantum mechanical nature of the electronic band gap, otherwise not accessible by classical descriptions. In detail, the Density Functional Theory has been selected as ab initio framework, thanks to its high efficiency in the calculation of the electron correlation effects in comparison to the Hartee Fock methods.

The results may be summarised as follows. The most significant changes in the band gap size can be achieved by the addition of a layer to a two-layered system, irrespective of the chemical composition. The cation substitution is not as effective as the number of layers in the determination of the value of the band gap; however, the induced variation is still significant, and therefore the doping can be used as a "knob" to finely tune the gap size. Similar subtle effect has been found for the position of the dopant in the 3-layer systems.

From the DOS analysis we understood that the cations play the major role in determining the electronic transition from the top of the valence band to the bottom of the conduction band, no matter if the compound is the pristine or the doped one. The composition of the bottom of the conduction band is the part of the electronic level spectrum that is affected the most by the cation substitution. The dopant atom hybridizes with both the native cation and the anion in such a way that the conduction band slightly contracts towards higher energies. We find a peculiar behaviour for the compounds containing the Te atom: the anion seems to mitigate the effect that the dopant has on the top of the valence band, hence on the width of the band gap.

The study of the covalent character of the atomic bonds, together with the analysis of the directionality of the electronic density in the cation environment would help to better clarify the role of the dopant in the determination of the band gap. This study is indeed already planned and constitutes an extension of the present work, which will lead to the identification of general guidelines to select suitable atomic types as dopant species to engineer the band gap in TMD-based heterostructures.

Chapter 5

Appendix

Here in the following, we report the optimised structures in cif format.

5.1 2L-MoS

```
data_findsym-output
  _audit_creation_method FINDSYM
  _symmetry_space_group_name_H-M "P -3 2/m 1"
  _symmetry_Int_Tables_number 164
  _cell_length_a 3.15604
  _cell_length_b 3.15604
  _cell_length_c 50.00000
  _cell_angle_alpha 90.00000
  _cell_angle_beta 90.00000
  _cell_angle_gamma 120.00000
  loop_ _space_group_symop_id
  _space_group_symop_operation_xyz
  1 x,y,z
  2 -y,x-y,z
  3 -x+y,-x,z
  4 x-y,-y,-z
  5 y,x,-z
  6 -x,-x+y,-z
  7 -x,-y,-z
  8 y,-x+y,-z
  9 x-y,x,-z
  10 -x+y,y,z
  11 -y,-x,z
  12 x,x-y,z
  loop_
  _atom_site_label
  _atom_site_type_symbol
  _atom_site_symmetry_multiplicity
  _atom_site_Wyckoff_label
  _atom_site_fract_x
```

_atom_site_fract_y
_atom_site_fract_z
_atom_site_occupancy
Mo1 Mo 2 d 0.33333 0.66667 0.06163 1.00000
S1 S 2 d 0.33333 0.66667 -0.03031 1.00000
S2 S 2 d 0.33333 0.66667 -0.09294 1.00000

5.2 2L-MoSe

data_findsym-output
_audit_creation_method FINDSYM
_symmetry_space_group_name_H-M "P -3 2/m 1"
_symmetry_Int_Tables_number 164
_cell_length_a 3.28445
_cell_length_b 3.28445
_cell_length_c 60.00000
_cell_angle_alpha 90.00000
_cell_angle_beta 90.00000
_cell_angle_gamma 120.00000
loop_
_space_group_symop_id
_space_group_symop_operation_xyz
1 x,y,z
2 -y,x-y,z
3 -x+y,-x,z
4 x-y,-y,-z
5 y,x,-z
6 -x,-x+y,-z
7 -x,-y,-z
8 y,-x+y,-z
9 x-y,x,-z
10 -x+y,y,z
11 -y,-x,z
12 x,x-y,z
loop_
_atom_site_label
_atom_site_type_symbol
_atom_site_symmetry_multiplicity
_atom_site_Wyckoff_label
_atom_site_fract_x
_atom_site_fract_y
_atom_site_fract_z
_atom_site_occupancy
Mo1 Mo 2 d 0.33333 0.66667 -0.05388 1.00000
Se1 Se 2 d 0.33333 0.66667 0.08180 1.00000
Se2 Se 2 d 0.33333 0.66667 0.02596 1.00000

5.3 2L-MoTe

```
data_findsym-output
  _audit_creation_method FINDSYM
  _symmetry_space_group_name_H-M "P -3 2/m 1"
  _symmetry_Int_Tables_number 164
  _cell_length_a 3.51814
  _cell_length_b 3.51814
  _cell_length_c 60.00000
  _cell_angle_alpha 90.00000
  _cell_angle_beta 90.00000
  _cell_angle_gamma 120.00000
  loop_
  _space_group_symop_id
  _space_group_symop_operation_xyz
  1 x,y,z
  2 -y,x-y,z
  3 -x+y,-x,z
  4 x-y,-y,-z
  5 y,x,-z
  6 -x,-x+y,-z
  7 -x,-y,-z
  8 y,-x+y,-z
  9 x-y,x,-z
  10 -x+y,y,z
  11 -y,-x,z
  12 x,x-y,z
  loop_
  _atom_site_label
  _atom_site_type_symbol
  _atom_site_symmetry_multiplicity
  _atom_site_Wyckoff_label
  _atom_site_fract_x
  _atom_site_fract_y
  _atom_site_fract_z
  _atom_site_occupancy
  Mo1 Mo 2 d 0.33333 0.66667 -0.05767 1.00000
  Te1 Te 2 d 0.33333 0.66667 0.08798 1.00000
  Te2 Te 2 d 0.33333 0.66667 0.02732 1.00000
```

5.4 2L-WS

```
data_findsym-output
  _audit_creation_method FINDSYM
  _symmetry_space_group_name_H-M "P -3 2/m 1"
```

_symmetry_Int_Tables_number 164
_cell_length_a 3.15992
_cell_length_b 3.15992
_cell_length_c 60.00000
_cell_angle_alpha 90.00000
_cell_angle_beta 90.00000
_cell_angle_gamma 120.00000
loop_
_space_group_symop_id
_space_group_symop_operation_xyz
1 x,y,z
2 -y,x-y,z
3 -x+y,-x,z
4 x-y,-y,-z
5 y,x,-z
6 -x,-x+y,-z
7 -x,-y,-z
8 y,-x+y,-z
9 x-y,x,-z
10 -x+y,y,z
11 -y,-x,z
12 x,x-y,z
loop_
_atom_site_label
_atom_site_type_symbol
_atom_site_symmetry_multiplicity
_atom_site_Wyckoff_label
_atom_site_fract_x
_atom_site_fract_y
_atom_site_fract_z
_atom_site_occupancy
W1 W 2 d 0.33333 0.66667 -0.05108 1.00000
S1 S 2 d 0.33333 0.66667 0.07735 1.00000
S2 S 2 d 0.33333 0.66667 0.02483 1.00000

5.5 2L-WSe

data_findsym-output
_audit_creation_method FINDSYM
_symmetry_space_group_name_H-M "P -3 2/m 1"
_symmetry_Int_Tables_number 164
_cell_length_a 3.28762
_cell_length_b 3.28762
_cell_length_c 60.00000
_cell_angle_alpha 90.00000
_cell_angle_beta 90.00000

_cell_angle_gamma 120.00000
loop_
_space_group_symop_id
_space_group_symop_operation_xyz
1 x,y,z
2 -y,x-y,z
3 -x+y,-x,z
4 x-y,-y,-z
5 y,x,-z
6 -x,-x+y,-z
7 -x,-y,-z
8 y,-x+y,-z
9 x-y,x,-z
10 -x+y,y,z
11 -y,-x,z
12 x,x-y,z
loop_
_atom_site_label
_atom_site_type_symbol
_atom_site_symmetry_multiplicity
_atom_site_Wyckoff_label
_atom_site_fract_x
_atom_site_fract_y
_atom_site_fract_z
_atom_site_occupancy
W1 W 2 d 0.33333 0.66667 0.05394 1.00000
Se1 Se 2 d 0.33333 0.66667 -0.08203 1.00000
Se2 Se 2 d 0.33333 0.66667 -0.02585 1.00000

5.6 2L-WTe

data_findsym-output
_audit_creation_method FINDSYM
_symmetry_space_group_name_H-M "P -3 2/m 1"
_symmetry_Int_Tables_number 164
_cell_length_a 3.52116
_cell_length_b 3.52116
_cell_length_c 60.00000
_cell_angle_alpha 90.00000
_cell_angle_beta 90.00000
_cell_angle_gamma 120.00000
loop_
_space_group_symop_id
_space_group_symop_operation_xyz
1 x,y,z
2 -y,x-y,z

3 -x+y,-x,z
4 x-y,-y,-z
5 y,x,-z
6 -x,-x+y,-z
7 -x,-y,-z
8 y,-x+y,-z
9 x-y,x,-z
10 -x+y,y,z
11 -y,-x,z
12 x,x-y,z
loop_
_atom_site_label
_atom_site_type_symbol
_atom_site_symmetry_multiplicity
_atom_site_Wyckoff_label
_atom_site_fract_x
_atom_site_fract_y
_atom_site_fract_z
_atom_site_occupancy
W1 W 2 d 0.33333 0.66667 -0.05761 1.00000
Te1 Te 2 d 0.33333 0.66667 0.08805 1.00000
Te2 Te 2 d 0.33333 0.66667 0.02713 1.00000

5.7 W:2L-MoS

data_findsym-output
_audit_creation_method FINDSYM
_symmetry_space_group_name_H-M "P 3 m 1"
_symmetry_Int_Tables_number 156
_cell_length_a 6.31462
_cell_length_b 6.31462
_cell_length_c 60.00000
_cell_angle_alpha 90.00000
_cell_angle_beta 90.00000
_cell_angle_gamma 120.00000
loop_
_space_group_symop_id
_space_group_symop_operation_xyz
1 x,y,z
2 -y,x-y,z
3 -x+y,-x,z
4 -x+y,y,z
5 -y,-x,z
6 x,x-y,z
loop_
_atom_site_label

_atom_site_type_symbol
_atom_site_symmetry_multiplicity
_atom_site_Wyckoff_label
_atom_site_fract_x
_atom_site_fract_y
_atom_site_fract_z
_atom_site_occupancy
Mo1 Mo 3 d 0.50001 0.49999 0.84654 1.00000
Mo2 Mo 3 d 0.83376 0.16624 -0.05145 1.00000
Mo3 Mo 1 a 0.00000 0.00000 0.84653 1.00000
W1 W 1 b 0.33333 0.66667 -0.05147 1.00000
S1 S 1 b 0.33333 0.66667 0.87262 1.00000
S2 S 3 d 0.83337 0.16663 0.87261 1.00000
S3 S 3 d 0.50003 0.49997 -0.07758 1.00000
S4 S 1 a 0.00000 0.00000 -0.07756 1.00000
S5 S 3 d 0.50001 0.49999 -0.02531 1.00000
S6 S 1 a 0.00000 0.00000 -0.02532 1.00000
S7 S 1 b 0.33333 0.66667 0.82044 1.00000
S8 S 3 d 0.83334 0.16666 0.82044 1.00000

5.8 W:2L-MoSe

data_findsym-output
_audit_creation_method FINDSYM
_symmetry_space_group_name_H-M "P 3 m 1"
_symmetry_Int_Tables_number 156
_cell_length_a 6.57034
_cell_length_b 6.57034
_cell_length_c 60.00000
_cell_angle_alpha 90.00000
_cell_angle_beta 90.00000
_cell_angle_gamma 120.00000
loop_
_space_group_symop_id
_space_group_symop_operation_xyz
1 x,y,z
2 -y,x-y,z
3 -x+y,-x,z
4 -x+y,y,z
5 -y,-x,z
6 x,x-y,z
loop_
_atom_site_label
_atom_site_type_symbol
_atom_site_symmetry_multiplicity
_atom_site_Wyckoff_label

_atom_site_fract_x
_atom_site_fract_y
_atom_site_fract_z
_atom_site_occupancy
Mo1 Mo 1 a 0.00000 0.00000 0.83834 1.00000
Mo2 Mo 3 d 0.83369 0.16631 -0.05385 1.00000
Mo3 Mo 3 d 0.50000 0.50000 0.83835 1.00000
W1 W 1 b 0.33333 0.66667 -0.05385 1.00000
Se1 Se 3 d 0.50017 0.49983 -0.02589 1.00000
Se2 Se 1 a 0.00000 0.00000 -0.02589 1.00000
Se3 Se 3 d 0.50016 0.49984 -0.08181 1.00000
Se4 Se 1 a 0.00000 0.00000 -0.08181 1.00000
Se5 Se 1 b 0.33333 0.66667 0.86627 1.00000
Se6 Se 3 d 0.83335 0.16665 0.86626 1.00000
Se7 Se 1 b 0.33333 0.66667 0.81044 1.00000
Se8 Se 3 d 0.83333 0.16667 0.81044 1.00000

5.9 W:2L-MoTe

data_findsym-output
_audit_creation_method FINDSYM
_symmetry_space_group_name_H-M "P 3 m 1"
_symmetry_Int_Tables_number 156
_cell_length_a 7.03932
_cell_length_b 7.03932
_cell_length_c 60.00000
_cell_angle_alpha 90.00000
_cell_angle_beta 90.00000
_cell_angle_gamma 120.00000
loop_
_space_group_symop_id
_space_group_symop_operation_xyz
1 x,y,z
2 -y,x-y,z
3 -x+y,-x,z
4 -x+y,y,z
5 -y,-x,z
6 x,x-y,z
loop_
_atom_site_label
_atom_site_type_symbol
_atom_site_symmetry_multiplicity
_atom_site_Wyckoff_label
_atom_site_fract_x
_atom_site_fract_y
_atom_site_fract_z

_atom_site_occupancy
Mo1 Mo 1 c 0.66667 0.33333 0.17386 1.00000
Mo2 Mo 3 d 0.50027 0.49973 0.05864 1.00000
Mo3 Mo 3 d 0.16666 0.83334 0.17384 1.00000
W1 W 1 a 0.00000 0.00000 0.05866 1.00000
Te1 Te 3 d 0.16700 0.83300 0.02832 1.00000
Te2 Te 1 c 0.66667 0.33333 0.02830 1.00000
Te3 Te 3 d 0.16700 0.83300 0.08901 1.00000
Te4 Te 1 c 0.66667 0.33333 0.08903 1.00000
Te5 Te 1 a 0.00000 0.00000 0.14349 1.00000
Te6 Te 3 d 0.50004 0.49996 0.14350 1.00000
Te7 Te 1 a 0.00000 0.00000 0.20413 1.00000
Te8 Te 3 d 0.49998 0.50002 0.20414 1.00000

5.10 Mo:2L-WS

data_findsym-output
_audit_creation_method FINDSYM
_symmetry_space_group_name_H-M "P 3 m 1"
_symmetry_Int_Tables_number 156
_cell_length_a 6.31954
_cell_length_b 6.31954
_cell_length_c 60.00000
_cell_angle_alpha 90.00000
_cell_angle_beta 90.00000
_cell_angle_gamma 120.00000
loop_
_space_group_symop_id
_space_group_symop_operation_xyz
1 x,y,z
2 -y,x-y,z
3 -x+y,-x,z
4 -x+y,y,z
5 -y,-x,z
6 x,x-y,z
loop_
_atom_site_label
_atom_site_type_symbol
_atom_site_symmetry_multiplicity
_atom_site_Wyckoff_label
_atom_site_fract_x
_atom_site_fract_y
_atom_site_fract_z
_atom_site_occupancy
W1 W 1 a 0.00000 0.00000 0.15379 1.00000
W2 W 3 d 0.83285 0.16715 0.05159 1.00000

W3 W 3 d 0.50000 0.50000 0.15379 1.00000
Mo1 Mo 1 b 0.33333 0.66667 0.05157 1.00000
S1 S 3 d 0.49998 0.50002 0.02536 1.00000
S2 S 1 a 0.00000 0.00000 0.02538 1.00000
S3 S 3 d 0.49994 0.50006 0.07779 1.00000
S4 S 1 a 0.00000 0.00000 0.07778 1.00000
S5 S 1 b 0.33333 0.66667 0.12754 1.00000
S6 S 3 d 0.83332 0.16668 0.12754 1.00000
S7 S 1 b 0.33333 0.66667 0.18008 1.00000
S8 S 3 d 0.83334 0.16666 0.18007 1.00000

5.11 Mo:2L-WSe

data_findsym-output
_audit_creation_method FINDSYM
_symmetry_space_group_name_H-M "P 3 m 1"
_symmetry_Int_Tables_number 156
_cell_length_a 6.57513
_cell_length_b 6.57513
_cell_length_c 60.00000
_cell_angle_alpha 90.00000
_cell_angle_beta 90.00000
_cell_angle_gamma 120.00000
loop_
_space_group_symop_id
_space_group_symop_operation_xyz
1 x,y,z
2 -y,x-y,z
3 -x+y,-x,z
4 -x+y,y,z
5 -y,-x,z
6 x,x-y,z
loop_
_atom_site_label
_atom_site_type_symbol
_atom_site_symmetry_multiplicity
_atom_site_Wyckoff_label
_atom_site_fract_x
_atom_site_fract_y
_atom_site_fract_z
_atom_site_occupancy
W1 W 1 c 0.66667 0.33333 0.16215 1.00000
W2 W 3 d 0.83384 0.16616 0.05419 1.00000
W3 W 3 d 0.16667 0.83333 0.16216 1.00000
Mo1 Mo 1 b 0.33333 0.66667 0.05414 1.00000
Se1 Se 3 d 0.16681 0.83319 0.02613 1.00000

Se2 Se 1 c 0.66667 0.33333 0.02617 1.00000
Se3 Se 3 d 0.16692 0.83308 0.08222 1.00000
Se4 Se 1 c 0.66667 0.33333 0.08220 1.00000
Se5 Se 1 b 0.33333 0.66667 0.13407 1.00000
Se6 Se 3 d 0.83335 0.16665 0.13407 1.00000
Se7 Se 1 b 0.33333 0.66667 0.19025 1.00000
Se8 Se 3 d 0.83333 0.16667 0.19025 1.00000

5.12 Mo:2L-WTe

data_findsym-output
_audit_creation_method FINDSYM
_symmetry_space_group_name_H-M "P 3 m 1"
_symmetry_Int_Tables_number 156
_cell_length_a 7.04298
_cell_length_b 7.04298
_cell_length_c 59.99863
_cell_angle_alpha 90.00000
_cell_angle_beta 90.00000
_cell_angle_gamma 120.00000
loop_
_space_group_symop_id
_space_group_symop_operation_xyz
1 x,y,z
2 -y,x-y,z
3 -x+y,-x,z
4 -x+y,y,z
5 -y,-x,z
6 x,x-y,z
loop_
_atom_site_label
_atom_site_type_symbol
_atom_site_symmetry_multiplicity
_atom_site_Wyckoff_label
_atom_site_fract_x
_atom_site_fract_y
_atom_site_fract_z
_atom_site_occupancy
W1 W 3 d 0.83283 0.16717 0.06166 1.00000
W2 W 3 d 0.49999 0.50001 0.17685 1.00000
W3 W 1 a 0.00000 0.00000 0.17684 1.00000
Mo1 Mo 1 b 0.33333 0.66667 0.06165 1.00000
Te1 Te 3 d 0.49963 0.50037 0.03124 1.00000
Te2 Te 1 a 0.00000 0.00000 0.03131 1.00000
Te3 Te 3 d 0.49962 0.50038 0.09210 1.00000
Te4 Te 1 a 0.00000 0.00000 0.09204 1.00000

Te5 Te 1 b 0.33333 0.66667 0.14637 1.00000
Te6 Te 3 d 0.83332 0.16668 0.14636 1.00000
Te7 Te 1 b 0.33333 0.66667 0.20729 1.00000
Te8 Te 3 d 0.83333 0.16667 0.20729 1.00000

5.13 3L-MoS

data_findsym-output
_audit_creation_method FINDSYM
_symmetry_space_group_name_H-M "P -6 m 2"
_symmetry_Int_Tables_number 187
_cell_length_a 3.15614
_cell_length_b 3.15614
_cell_length_c 70.00000
_cell_angle_alpha 90.00000
_cell_angle_beta 90.00000
_cell_angle_gamma 120.00000
loop_
_space_group_symop_id
_space_group_symop_operation_xyz
1 x,y,z
2 -y,x-y,z
3 -x+y,-x,z
4 x,x-y,-z
5 -x+y,y,-z
6 -y,-x,-z
7 -x+y,-x,-z
8 x,y,-z
9 -y,x-y,-z
10 -x+y,y,z
11 -y,-x,z
12 x,x-y,z
loop_
_atom_site_label
_atom_site_type_symbol
_atom_site_symmetry_multiplicity
_atom_site_Wyckoff_label
_atom_site_fract_x
_atom_site_fract_y
_atom_site_fract_z
_atom_site_occupancy
Mo1 Mo 2 h 0.33333 0.66667 -0.08776 1.00000
Mo2 Mo 1 e 0.66667 0.33333 0.00000 1.00000
S1 S 2 h 0.33333 0.66667 -0.02236 1.00000
S2 S 2 i 0.66667 0.33333 0.06539 1.00000
S3 S 2 i 0.66667 0.33333 0.11013 1.00000

5.14 3L-MoSe

```
data_findsym-output
  _audit_creation_method FINDSYM
  _symmetry_space_group_name_H-M "P -6 m 2"
  _symmetry_Int_Tables_number 187
  _cell_length_a 3.28423
  _cell_length_b 3.28423
  _cell_length_c 70.00000
  _cell_angle_alpha 90.00000
  _cell_angle_beta 90.00000
  _cell_angle_gamma 120.00000
  loop_
  _space_group_symop_id
  _space_group_symop_operation_xyz
  1 x,y,z
  2 -y,x-y,z
  3 -x+y,-x,z
  4 x,x-y,-z
  5 -x+y,y,-z
  6 -y,-x,-z
  7 -x+y,-x,-z
  8 x,y,-z
  9 -y,x-y,-z
  10 -x+y,y,z
  11 -y,-x,z
  12 x,x-y,z
  loop_
  _atom_site_label
  _atom_site_type_symbol
  _atom_site_symmetry_multiplicity
  _atom_site_Wyckoff_label
  _atom_site_fract_x
  _atom_site_fract_y
  _atom_site_fract_z
  _atom_site_occupancy
  Mo1 Mo 2 h 0.33333 0.66667 -0.09251 1.00000
  Mo2 Mo 1 e 0.66667 0.33333 0.00000 1.00000
  Se1 Se 2 i 0.66667 0.33333 0.88357 1.00000
  Se2 Se 2 i 0.66667 0.33333 -0.06857 1.00000
  Se3 Se 2 h 0.33333 0.66667 -0.02394 1.00000
```

5.15 3L-MoTe

```
data_findsym-output
```

_audit_creation_method FINDSYM
_symmetry_space_group_name_H-M "P -6 m 2"
_symmetry_Int_Tables_number 187
_cell_length_a 3.51816
_cell_length_b 3.51816
_cell_length_c 70.00000
_cell_angle_alpha 90.00000
_cell_angle_beta 90.00000
_cell_angle_gamma 120.00000
loop_
_space_group_symop_id
_space_group_symop_operation_xyz
1 x,y,z
2 -y,x-y,z
3 -x+y,-x,z
4 x,x-y,-z
5 -x+y,y,-z
6 -y,-x,-z
7 -x+y,-x,-z
8 x,y,-z
9 -y,x-y,-z
10 -x+y,y,z
11 -y,-x,z
12 x,x-y,z
loop_
_atom_site_label
_atom_site_type_symbol
_atom_site_symmetry_multiplicity
_atom_site_Wyckoff_label
_atom_site_fract_x
_atom_site_fract_y
_atom_site_fract_z
_atom_site_occupancy
Mo1 Mo 2 h 0.33333 0.66667 -0.09894 1.00000
Mo2 Mo 1 e 0.66667 0.33333 0.00000 1.00000
Te1 Te 2 i 0.66667 0.33333 0.87509 1.00000
Te2 Te 2 i 0.66667 0.33333 -0.07291 1.00000
Te3 Te 2 h 0.33333 0.66667 -0.02600 1.00000

5.16 3L-WS

data_findsym-output
_audit_creation_method FINDSYM
_symmetry_space_group_name_H-M "P -6 m 2"
_symmetry_Int_Tables_number 187
_cell_length_a 3.15988

_cell_length_b 3.15988
_cell_length_c 70.00000
_cell_angle_alpha 90.00000
_cell_angle_beta 90.00000
_cell_angle_gamma 120.00000
loop_
_space_group_symop_id
_space_group_symop_operation_xyz
1 x,y,z
2 -y,x-y,z
3 -x+y,-x,z
4 x,x-y,-z
5 -x+y,y,-z
6 -y,-x,-z
7 -x+y,-x,-z
8 x,y,-z
9 -y,x-y,-z
10 -x+y,y,z
11 -y,-x,z
12 x,x-y,z
loop_
_atom_site_label
_atom_site_type_symbol
_atom_site_symmetry_multiplicity
_atom_site_Wyckoff_label
_atom_site_fract_x
_atom_site_fract_y
_atom_site_fract_z
_atom_site_occupancy
W1 W 2 h 0.33333 0.66667 -0.08739 1.00000
W2 W 1 e 0.66667 0.33333 0.00000 1.00000
S1 S 2 i 0.66667 0.33333 0.89009 1.00000
S2 S 2 i 0.66667 0.33333 -0.06489 1.00000
S3 S 2 h 0.33333 0.66667 -0.02250 1.00000

5.17 3L-WSe

data_findsym-output
_audit_creation_method FINDSYM
_symmetry_space_group_name_H-M "P -6 m 2"
_symmetry_Int_Tables_number 187
_cell_length_a 3.28767
_cell_length_b 3.28767
_cell_length_c 70.00000
_cell_angle_alpha 90.00000
_cell_angle_beta 90.00000

_cell_angle_gamma 120.00000
loop_
_space_group_symop_id
_space_group_symop_operation_xyz
1 x,y,z
2 -y,x-y,z
3 -x+y,-x,z
4 x,x-y,-z
5 -x+y,y,-z
6 -y,-x,-z
7 -x+y,-x,-z
8 x,y,-z
9 -y,x-y,-z
10 -x+y,y,z
11 -y,-x,z
12 x,x-y,z
loop_
_atom_site_label
_atom_site_type_symbol
_atom_site_symmetry_multiplicity
_atom_site_Wyckoff_label
_atom_site_fract_x
_atom_site_fract_y
_atom_site_fract_z
_atom_site_occupancy
W1 W 2 i 0.66667 0.33333 -0.09232 1.00000
W2 W 1 c 0.33333 0.66667 0.00000 1.00000
Se1 Se 2 h 0.33333 0.66667 0.88361 1.00000
Se2 Se 2 h 0.33333 0.66667 -0.06825 1.00000
Se3 Se 2 i 0.66667 0.33333 -0.02407 1.00000

5.18 3L-WTe

data_findsym-output
_audit_creation_method FINDSYM
_symmetry_space_group_name_H-M "P -6 m 2"
_symmetry_Int_Tables_number 187
_cell_length_a 3.52073
_cell_length_b 3.52073
_cell_length_c 70.00000
_cell_angle_alpha 90.00000
_cell_angle_beta 90.00000
_cell_angle_gamma 120.00000
loop_
_space_group_symop_id
_space_group_symop_operation_xyz

1 x,y,z
2 -y,x-y,z
3 -x+y,-x,z
4 x,x-y,-z
5 -x+y,y,-z
6 -y,-x,-z
7 -x+y,-x,-z
8 x,y,-z
9 -y,x-y,-z
10 -x+y,y,z
11 -y,-x,z
12 x,x-y,z
loop_
_atom_site_label
_atom_site_type_symbol
_atom_site_symmetry_multiplicity
_atom_site_Wyckoff_label
_atom_site_fract_x
_atom_site_fract_y
_atom_site_fract_z
_atom_site_occupancy
W1 W 2 h 0.33333 0.66667 -0.09878 1.00000
W2 W 1 e 0.66667 0.33333 0.00000 1.00000
Te1 Te 2 i 0.66667 0.33333 0.87512 1.00000
Te2 Te 2 i 0.66667 0.33333 -0.07265 1.00000
Te3 Te 2 h 0.33333 0.66667 -0.02611 1.00000

5.19 W:3L-L1-MoS

data_findsym-output
_audit_creation_method FINDSYM
_symmetry_space_group_name_H-M "P 3 m 1"
_symmetry_Int_Tables_number 156
_cell_length_a 6.31400
_cell_length_b 6.31400
_cell_length_c 70.00000
_cell_angle_alpha 90.00000
_cell_angle_beta 90.00000
_cell_angle_gamma 120.00000
loop_
_space_group_symop_id
_space_group_symop_operation_xyz
1 x,y,z
2 -y,x-y,z
3 -x+y,-x,z
4 -x+y,y,z

5 -y,-x,z
6 x,x-y,z
loop_
_atom_site_label
_atom_site_type_symbol
_atom_site_symmetry_multiplicity
_atom_site_Wyckoff_label
_atom_site_fract_x
_atom_site_fract_y
_atom_site_fract_z
_atom_site_occupancy
Mo1 Mo 3 d 0.16707 0.83293 -0.04422 1.00000
Mo2 Mo 3 d 0.83335 0.16665 0.86814 1.00000
Mo3 Mo 1 b 0.33333 0.66667 0.86814 1.00000
Mo4 Mo 1 c 0.66667 0.33333 0.78090 1.00000
Mo5 Mo 3 d 0.16666 0.83334 0.78090 1.00000
W1 W 1 c 0.66667 0.33333 -0.04424 1.00000
S1 S 1 c 0.66667 0.33333 0.89049 1.00000
S2 S 3 d 0.16669 0.83331 0.89049 1.00000
S3 S 3 d 0.83334 0.16666 0.80324 1.00000
S4 S 1 b 0.33333 0.66667 0.80324 1.00000
S5 S 3 d 0.83333 0.16667 0.75853 1.00000
S6 S 1 b 0.33333 0.66667 0.75853 1.00000
S7 S 3 d 0.83338 0.16662 -0.06663 1.00000
S8 S 1 b 0.33333 0.66667 -0.06661 1.00000
S9 S 3 d 0.83332 0.16668 -0.02182 1.00000
S10 S 1 b 0.33333 0.66667 -0.02182 1.00000
S11 S 1 c 0.66667 0.33333 0.84579 1.00000
S12 S 3 d 0.16666 0.83334 0.84579 1.00000

5.20 W:3L-L1-MoSe

data_findsym-output
_audit_creation_method FINDSYM
_symmetry_space_group_name_H-M "P 3 m 1"
_symmetry_Int_Tables_number 156
_cell_length_a 6.56958
_cell_length_b 6.56958
_cell_length_c 70.00000
_cell_angle_alpha 90.00000
_cell_angle_beta 90.00000
_cell_angle_gamma 120.00000
loop_
_space_group_symop_id
_space_group_symop_operation_xyz
1 x,y,z

2 -y,x-y,z
3 -x+y,-x,z
4 -x+y,y,z
5 -y,-x,z
6 x,x-y,z
loop_
_atom_site_label
_atom_site_type_symbol
_atom_site_symmetry_multiplicity
_atom_site_Wyckoff_label
_atom_site_fract_x
_atom_site_fract_y
_atom_site_fract_z
_atom_site_occupancy
Mo1 Mo 3 d 0.16703 0.83297 -0.04604 1.00000
Mo2 Mo 3 d 0.83335 0.16665 0.86154 1.00000
Mo3 Mo 1 b 0.33333 0.66667 0.86155 1.00000
Mo4 Mo 1 c 0.66667 0.33333 0.76889 1.00000
Mo5 Mo 3 d 0.16667 0.83333 0.76889 1.00000
W1 W 1 c 0.66667 0.33333 -0.04604 1.00000
Se1 Se 3 d 0.83353 0.16647 -0.02208 1.00000
Se2 Se 1 b 0.33333 0.66667 -0.02208 1.00000
Se3 Se 3 d 0.83348 0.16652 -0.07001 1.00000
Se4 Se 1 b 0.33333 0.66667 -0.07002 1.00000
Se5 Se 1 c 0.66667 0.33333 0.88547 1.00000
Se6 Se 3 d 0.16666 0.83334 0.88548 1.00000
Se7 Se 1 c 0.66667 0.33333 0.83761 1.00000
Se8 Se 3 d 0.16669 0.83331 0.83761 1.00000
Se9 Se 3 d 0.83333 0.16667 0.79283 1.00000
Se10 Se 1 b 0.33333 0.66667 0.79283 1.00000
Se11 Se 3 d 0.83333 0.16667 0.74497 1.00000
Se12 Se 1 b 0.33333 0.66667 0.74496 1.00000

5.21 W:3L-L1-MoTe

data_findsym-output
_audit_creation_method FINDSYM
_symmetry_space_group_name_H-M "P 3 m 1"
_symmetry_Int_Tables_number 156
_cell_length_a 7.03718
_cell_length_b 7.03718
_cell_length_c 70.00000
_cell_angle_alpha 90.00000
_cell_angle_beta 90.00000
_cell_angle_gamma 120.00000
loop_

_space_group_symop_id
_space_group_symop_operation_xyz
1 x,y,z
2 -y,x-y,z
3 -x+y,-x,z
4 -x+y,y,z
5 -y,-x,z
6 x,x-y,z
loop_
_atom_site_label
_atom_site_type_symbol
_atom_site_symmetry_multiplicity
_atom_site_Wyckoff_label
_atom_site_fract_x
_atom_site_fract_y
_atom_site_fract_z
_atom_site_occupancy
Mo1 Mo 3 d 0.83335 0.16665 0.75176 1.00000
Mo2 Mo 3 d 0.83363 0.16637 -0.05066 1.00000
Mo3 Mo 3 d 0.49999 0.50001 0.85055 1.00000
Mo4 Mo 1 a 0.00000 0.00000 0.85055 1.00000
Mo5 Mo 1 b 0.33333 0.66667 0.75173 1.00000
W1 W 1 b 0.33333 0.66667 -0.05068 1.00000
Te1 Te 3 d 0.50032 0.49968 -0.02467 1.00000
Te2 Te 1 a 0.00000 0.00000 -0.02465 1.00000
Te3 Te 3 d 0.50033 0.49967 -0.07671 1.00000
Te4 Te 1 a 0.00000 0.00000 -0.07672 1.00000
Te5 Te 1 b 0.33333 0.66667 0.87655 1.00000
Te6 Te 3 d 0.83336 0.16664 0.87654 1.00000
Te7 Te 1 b 0.33333 0.66667 0.82456 1.00000
Te8 Te 3 d 0.83332 0.16668 0.82455 1.00000
Te9 Te 3 d 0.49996 0.50004 0.77777 1.00000
Te10 Te 1 a 0.00000 0.00000 0.77779 1.00000
Te11 Te 3 d 0.50005 0.49995 0.72578 1.00000
Te12 Te 1 a 0.00000 0.00000 0.72579 1.00000

5.22 Mo:3L-L1-WS

data_findsym-output
_audit_creation_method FINDSYM
_symmetry_space_group_name_H-M "P 3 m 1"
_symmetry_Int_Tables_number 156
_cell_length_a 6.31932
_cell_length_b 6.31932
_cell_length_c 70.00000
_cell_angle_alpha 90.00000

```
_cell_angle_beta 90.00000
_cell_angle_gamma 120.00000
loop_
_space_group_symop_id
_space_group_symop_operation_xyz
1 x,y,z
2 -y,x-y,z
3 -x+y,-x,z
4 -x+y,y,z
5 -y,-x,z
6 x,x-y,z
loop_
_atom_site_label
_atom_site_type_symbol
_atom_site_symmetry_multiplicity
_atom_site_Wyckoff_label
_atom_site_fract_x
_atom_site_fract_y
_atom_site_fract_z
_atom_site_occupancy
W1 W 3 d 0.16667 0.83333 0.78058 1.00000
W2 W 3 d 0.16618 0.83382 -0.04465 1.00000
W3 W 3 d 0.83333 0.16667 0.86796 1.00000
W4 W 1 b 0.33333 0.66667 0.86797 1.00000
W5 W 1 c 0.66667 0.33333 0.78058 1.00000
Mo1 Mo 1 c 0.66667 0.33333 -0.04463 1.00000
S1 S 3 d 0.83332 0.16668 -0.02216 1.00000
S2 S 1 b 0.33333 0.66667 -0.02218 1.00000
S3 S 3 d 0.83327 0.16673 -0.06710 1.00000
S4 S 1 b 0.33333 0.66667 -0.06709 1.00000
S5 S 1 c 0.66667 0.33333 0.89046 1.00000
S6 S 3 d 0.16665 0.83335 0.89046 1.00000
S7 S 1 c 0.66667 0.33333 0.84547 1.00000
S8 S 3 d 0.16667 0.83333 0.84547 1.00000
S9 S 3 d 0.83333 0.16667 0.80308 1.00000
S10 S 1 b 0.33333 0.66667 0.80308 1.00000
S11 S 3 d 0.83333 0.16667 0.75806 1.00000
S12 S 1 b 0.33333 0.66667 0.75806 1.00000
```

5.23 Mo:3L-L1-WSe

```
data_findsym-output
_audit_creation_method FINDSYM
_symmetry_space_group_name_H-M "P 3 m 1"
_symmetry_Int_Tables_number 156
_cell_length_a 6.57533
```

_cell_length_b 6.57533
_cell_length_c 70.00000
_cell_angle_alpha 90.00000
_cell_angle_beta 90.00000
_cell_angle_gamma 120.00000
loop_
_space_group_symop_id
_space_group_symop_operation_xyz
1 x,y,z
2 -y,x-y,z
3 -x+y,-x,z
4 -x+y,y,z
5 -y,-x,z
6 x,x-y,z
loop_
_atom_site_label
_atom_site_type_symbol
_atom_site_symmetry_multiplicity
_atom_site_Wyckoff_label
_atom_site_fract_x
_atom_site_fract_y
_atom_site_fract_z
_atom_site_occupancy
W1 W 3 d 0.83333 0.16667 0.23142 1.00000
W2 W 3 d 0.83384 0.16616 0.04673 1.00000
W3 W 3 d 0.16667 0.83333 0.13907 1.00000
W4 W 1 c 0.66667 0.33333 0.13907 1.00000
W5 W 1 b 0.33333 0.66667 0.23142 1.00000
Mo1 Mo 1 b 0.33333 0.66667 0.04672 1.00000
Se1 Se 3 d 0.16685 0.83315 0.02269 1.00000
Se2 Se 1 c 0.66667 0.33333 0.02272 1.00000
Se3 Se 3 d 0.16687 0.83313 0.07076 1.00000
Se4 Se 1 c 0.66667 0.33333 0.07073 1.00000
Se5 Se 1 b 0.33333 0.66667 0.11500 1.00000
Se6 Se 3 d 0.83335 0.16665 0.11500 1.00000
Se7 Se 1 b 0.33333 0.66667 0.16314 1.00000
Se8 Se 3 d 0.83333 0.16667 0.16314 1.00000
Se9 Se 3 d 0.16666 0.83334 0.20735 1.00000
Se10 Se 1 c 0.66667 0.33333 0.20735 1.00000
Se11 Se 3 d 0.16667 0.83333 0.25549 1.00000
Se12 Se 1 c 0.66667 0.33333 0.25549 1.00000

5.24 Mo:3L-L1-WTe

data_findsym-output
_audit_creation_method FINDSYM

_symmetry_space_group_name_H-M "P 3 m 1"
_symmetry_Int_Tables_number 156
_cell_length_a 7.04172
_cell_length_b 7.04172
_cell_length_c 70.00000
_cell_angle_alpha 90.00000
_cell_angle_beta 90.00000
_cell_angle_gamma 120.00000
loop_
_space_group_symop_id
_space_group_symop_operation_xyz
1 x,y,z
2 -y,x-y,z
3 -x+y,-x,z
4 -x+y,y,z
5 -y,-x,z
6 x,x-y,z
loop_
_atom_site_label
_atom_site_type_symbol
_atom_site_symmetry_multiplicity
_atom_site_Wyckoff_label
_atom_site_fract_x
_atom_site_fract_y
_atom_site_fract_z
_atom_site_occupancy
W1 W 3 d 0.16666 0.83334 0.25210 1.00000
W2 W 3 d 0.16619 0.83381 0.05455 1.00000
W3 W 3 d 0.83333 0.16667 0.15332 1.00000
W4 W 1 b 0.33333 0.66667 0.15332 1.00000
W5 W 1 c 0.66667 0.33333 0.25210 1.00000
Mo1 Mo 1 c 0.66667 0.33333 0.05453 1.00000
Te1 Te 3 d 0.83297 0.16703 0.02847 1.00000
Te2 Te 1 b 0.33333 0.66667 0.02852 1.00000
Te3 Te 3 d 0.83296 0.16704 0.08064 1.00000
Te4 Te 1 b 0.33333 0.66667 0.08060 1.00000
Te5 Te 1 c 0.66667 0.33333 0.12721 1.00000
Te6 Te 3 d 0.16665 0.83335 0.12721 1.00000
Te7 Te 1 c 0.66667 0.33333 0.17943 1.00000
Te8 Te 3 d 0.16667 0.83333 0.17943 1.00000
Te9 Te 3 d 0.83333 0.16667 0.22597 1.00000
Te10 Te 1 b 0.33333 0.66667 0.22597 1.00000
Te11 Te 3 d 0.83333 0.16667 0.27820 1.00000
Te12 Te 1 b 0.33333 0.66667 0.27820 1.00000

5.25 W:3L-L2-MoS

data_findsym-output
_audit_creation_method FINDSYM
_symmetry_space_group_name_H-M "P -6 m 2"
_symmetry_Int_Tables_number 187
_cell_length_a 6.30945
_cell_length_b 6.30945
_cell_length_c 70.00000
_cell_angle_alpha 90.00000
_cell_angle_beta 90.00000
_cell_angle_gamma 120.00000
loop_
_space_group_symop_id
_space_group_symop_operation_xyz
1 x,y,z
2 -y,x-y,z
3 -x+y,-x,z
4 x,x-y,-z
5 -x+y,y,-z
6 -y,-x,-z
7 -x+y,-x,-z
8 x,y,-z
9 -y,x-y,-z
10 -x+y,y,z
11 -y,-x,z
12 x,x-y,z
loop_
_atom_site_label
_atom_site_type_symbol
_atom_site_symmetry_multiplicity
_atom_site_Wyckoff_label
_atom_site_fract_x
_atom_site_fract_y
_atom_site_fract_z
_atom_site_occupancy
Mo1 Mo 6 n 0.83333 0.16667 -0.08770 1.00000
Mo2 Mo 2 h 0.33333 0.66667 -0.08770 1.00000
Mo3 Mo 3 j 0.49958 0.50042 0.00000 1.00000
W1 W 1 a 0.00000 0.00000 0.00000 1.00000
S1 S 6 n 0.83331 0.16669 -0.02240 1.00000
S2 S 2 h 0.33333 0.66667 -0.02239 1.00000
S3 S 2 g 0.00000 0.00000 0.06534 1.00000
S4 S 6 n 0.49998 0.50002 0.06534 1.00000
S5 S 2 g 0.00000 0.00000 0.11008 1.00000
S6 S 6 n 0.50001 0.49999 0.11008 1.00000

5.26 W:3L-L2-MoSe

```
data_findsym-output
  _audit_creation_method FINDSYM
  _symmetry_space_group_name_H-M "P -6 m 2"
  _symmetry_Int_Tables_number 187
  _cell_length_a 6.57017
  _cell_length_b 6.57017
  _cell_length_c 70.00000
  _cell_angle_alpha 90.00000
  _cell_angle_beta 90.00000
  _cell_angle_gamma 120.00000
  loop_
  _space_group_symop_id
  _space_group_symop_operation_xyz
  1 x,y,z
  2 -y,x-y,z
  3 -x+y,-x,z
  4 x,x-y,-z
  5 -x+y,y,-z
  6 -y,-x,-z
  7 -x+y,-x,-z
  8 x,y,-z
  9 -y,x-y,-z
  10 -x+y,y,z
  11 -y,-x,z
  12 x,x-y,z
  loop_
  _atom_site_label
  _atom_site_type_symbol
  _atom_site_symmetry_multiplicity
  _atom_site_Wyckoff_label
  _atom_site_fract_x
  _atom_site_fract_y
  _atom_site_fract_z
  _atom_site_occupancy
  Mo1 Mo 6 n 0.83334 0.16666 0.40793 1.00000
  Mo2 Mo 2 h 0.33333 0.66667 0.40793 1.00000
  Mo3 Mo 3 k 0.16713 0.83287 0.50000 1.00000
  W1 W 1 f 0.66667 0.33333 0.50000 1.00000
  Se1 Se 2 i 0.66667 0.33333 0.38401 1.00000
  Se2 Se 6 n 0.16666 0.83334 0.38401 1.00000
  Se3 Se 2 i 0.66667 0.33333 0.43185 1.00000
  Se4 Se 6 n 0.16669 0.83331 0.43185 1.00000
  Se5 Se 6 n 0.83351 0.16649 0.47604 1.00000
  Se6 Se 2 h 0.33333 0.66667 0.47602 1.00000
```

5.27 W:3L-L2-MoTe

data_findsym-output
_audit_creation_method FINDSYM
_symmetry_space_group_name_H-M "P -6 m 2"
_symmetry_Int_Tables_number 187
_cell_length_a 7.03812
_cell_length_b 7.03812
_cell_length_c 70.00000
_cell_angle_alpha 90.00000
_cell_angle_beta 90.00000
_cell_angle_gamma 120.00000
loop_
_space_group_symop_id
_space_group_symop_operation_xyz
1 x,y,z
2 -y,x-y,z
3 -x+y,-x,z
4 x,x-y,-z
5 -x+y,y,-z
6 -y,-x,-z
7 -x+y,-x,-z
8 x,y,-z
9 -y,x-y,-z
10 -x+y,y,z
11 -y,-x,z
12 x,x-y,z
loop_
_atom_site_label
_atom_site_type_symbol
_atom_site_symmetry_multiplicity
_atom_site_Wyckoff_label
_atom_site_fract_x
_atom_site_fract_y
_atom_site_fract_z
_atom_site_occupancy
Mo1 Mo 6 n 0.83335 0.16665 0.40121 1.00000
Mo2 Mo 2 h 0.33333 0.66667 0.40120 1.00000
Mo3 Mo 3 k 0.49964 0.50036 0.50000 1.00000
W1 W 1 b 0.00000 0.00000 0.50000 1.00000
Te1 Te 2 g 0.00000 0.00000 0.37524 1.00000
Te2 Te 6 n 0.50000 0.50000 0.37524 1.00000
Te3 Te 2 g 0.00000 0.00000 0.42723 1.00000
Te4 Te 6 n 0.49999 0.50001 0.42722 1.00000
Te5 Te 6 n 0.83300 0.16700 0.47398 1.00000
Te6 Te 2 h 0.33333 0.66667 0.47396 1.00000

5.28 Mo:3L-L2-WS

```
data_findsym-output
  _audit_creation_method FINDSYM
  _symmetry_space_group_name_H-M "P -6 m 2"
  _symmetry_Int_Tables_number 187
  _cell_length_a 6.32106
  _cell_length_b 6.32106
  _cell_length_c 70.00000
  _cell_angle_alpha 90.00000
  _cell_angle_beta 90.00000
  _cell_angle_gamma 120.00000
  loop_
  _space_group_symop_id
  _space_group_symop_operation_xyz
  1 x,y,z
  2 -y,x-y,z
  3 -x+y,-x,z
  4 x,x-y,-z
  5 -x+y,y,-z
  6 -y,-x,-z
  7 -x+y,-x,-z
  8 x,y,-z
  9 -y,x-y,-z
  10 -x+y,y,z
  11 -y,-x,z
  12 x,x-y,z
  loop_
  _atom_site_label
  _atom_site_type_symbol
  _atom_site_symmetry_multiplicity
  _atom_site_Wyckoff_label
  _atom_site_fract_x
  _atom_site_fract_y
  _atom_site_fract_z
  _atom_site_occupancy
  W1 W 6 n 0.83333 0.16667 0.41261 1.00000
  W2 W 2 h 0.33333 0.66667 0.41261 1.00000
  W3 W 3 k 0.16617 0.83383 0.50000 1.00000
  Mo1 Mo 1 f 0.66667 0.33333 0.50000 1.00000
  S1 S 2 i 0.66667 0.33333 0.39010 1.00000
  S2 S 6 n 0.16667 0.83333 0.39010 1.00000
  S3 S 2 i 0.66667 0.33333 0.43511 1.00000
  S4 S 6 n 0.16665 0.83335 0.43511 1.00000
  S5 S 6 n 0.83329 0.16671 0.47755 1.00000
  S6 S 2 h 0.33333 0.66667 0.47757 1.00000
```

5.29 Mo:3L-L2-WSe

data_findsym-output
_audit_creation_method FINDSYM
_symmetry_space_group_name_H-M "P -6 m 2"
_symmetry_Int_Tables_number 187
_cell_length_a 6.57088
_cell_length_b 6.57088
_cell_length_c 70.00000
_cell_angle_alpha 90.00000
_cell_angle_beta 90.00000
_cell_angle_gamma 120.00000
loop_
_space_group_symop_id
_space_group_symop_operation_xyz
1 x,y,z
2 -y,x-y,z
3 -x+y,-x,z
4 x,x-y,-z
5 -x+y,y,-z
6 -y,-x,-z
7 -x+y,-x,-z
8 x,y,-z
9 -y,x-y,-z
10 -x+y,y,z
11 -y,-x,z
12 x,x-y,z
loop_
_atom_site_label
_atom_site_type_symbol
_atom_site_symmetry_multiplicity
_atom_site_Wyckoff_label
_atom_site_fract_x
_atom_site_fract_y
_atom_site_fract_z
_atom_site_occupancy
W1 W 2 i 0.66667 0.33333 0.09232 1.00000
W2 W 6 n 0.16666 0.83334 -0.09232 1.00000
W3 W 3 j 0.49948 0.50052 0.00000 1.00000
Mo1 Mo 1 a 0.00000 0.00000 0.00000 1.00000
Se1 Se 2 g 0.00000 0.00000 0.88359 1.00000
Se2 Se 6 n 0.50000 0.50000 0.88359 1.00000
Se3 Se 2 g 0.00000 0.00000 -0.06823 1.00000
Se4 Se 6 n 0.49999 0.50001 -0.06823 1.00000
Se5 Se 6 n 0.16646 0.83354 -0.02404 1.00000
Se6 Se 2 i 0.66667 0.33333 -0.02401 1.00000

5.30 Mo:3L-L2-WTe

data_findsym-output
_audit_creation_method FINDSYM
_symmetry_space_group_name_H-M "P -6 m 2"
_symmetry_Int_Tables_number 187
_cell_length_a 7.03638
_cell_length_b 7.03638
_cell_length_c 70.00000
_cell_angle_alpha 90.00000
_cell_angle_beta 90.00000
_cell_angle_gamma 120.00000
loop_
_space_group_symop_id
_space_group_symop_operation_xyz
1 x,y,z
2 -y,x-y,z
3 -x+y,-x,z
4 x,x-y,-z
5 -x+y,y,-z
6 -y,-x,-z
7 -x+y,-x,-z
8 x,y,-z
9 -y,x-y,-z
10 -x+y,y,z
11 -y,-x,z
12 x,x-y,z
loop_
_atom_site_label
_atom_site_type_symbol
_atom_site_symmetry_multiplicity
_atom_site_Wyckoff_label
_atom_site_fract_x
_atom_site_fract_y
_atom_site_fract_z
_atom_site_occupancy
W1 W 6 n 0.83333 0.16667 -0.09874 1.00000
W2 W 2 h 0.33333 0.66667 -0.09874 1.00000
W3 W 3 j 0.50056 0.49944 0.00000 1.00000
Mo1 Mo 1 a 0.00000 0.00000 0.00000 1.00000
Te1 Te 2 g 0.00000 0.00000 0.87515 1.00000
Te2 Te 6 n 0.50000 0.50000 0.87514 1.00000
Te3 Te 2 g 0.00000 0.00000 -0.07260 1.00000
Te4 Te 6 n 0.50001 0.49999 -0.07259 1.00000
Te5 Te 6 n 0.83372 0.16628 -0.02610 1.00000
Te6 Te 2 h 0.33333 0.66667 -0.02603 1.00000

Bibliography

[1] W. Setyawan and S. Curtarolo, "High-throughput electronic band structure calculations: Challenges and tools," Computational Materials Science, vol. 49, no. 2, pp. 299 – 312, 2010.

[2] IUCr, International Tables for Crystallography, Volume A: Space Group Symmetry. International Tables for Crystallography, Dordrecht, Boston, London: Kluwer Academic Publishers, 5. revised edition ed., 2002.

[3] NASA, "Vital signs: Global temperature." https://climate.nasa.gov/vital-signs/global-temperature, 2021. Accessed: 2021-21-01.

[4] NASA, "Vital signs: Carbon dioxide." https://climate.nasa.gov/vital-signs/carbon-dioxide/, 2021. Accessed: 2021-21-01.

[5] H. Ritchie and M. Roser, "Co2 and greenhouse gas emissions," Our World in Data, 2017. https://ourworldindata.org/co2-and-other-greenhouse-gas-emissions.

[6] H. Ritchie and M. Roser, "Renewable energy," Our World in Data, 2020. https://ourworldindata.org/renewable-energy.

[7] European Comission, "Eu climate action and the european green deal." https://ec.europa.eu/clima/policies/eu-climate-action_en. Accessed: 2021-04-05.

[8] A. Wiedermann, M. Ladwig, C. Bergins, O. Bernstrauch, C. Herce-Fuente, and P. Jansohn, "Flexible power generation in a decarbonised europe." https://www.etip-snet.eu/wp-content/uploads/2020/03/WG3_WhitePaper_Flexible-Power-Generation-in-a-Decarbonised-Europe.pdf. Accessed: 2021-04-05.

[9] H. Wang, H. Feng, and J. Li, "Graphene and graphene-like layered transition metal dichalcogenides in energy conversion and storage," Small, vol. 10, no. 11, pp. 2165–2181, 2014.

[10] C. Sumesh, "Towards efficient photon management in nanostructured solar cells: Role of 2d layered transition metal dichalcogenide semiconductors," Solar Energy Materials and Solar Cells, vol. 192, pp. 16 – 23, 2019.

[11] M. Z. Iqbal, S. Alam, M. M. Faisal, and S. Khan, "Recent advancement in the performance of solar cells by incorporating transition metal dichalcogenides as counter electrode and photoabsorber," International Journal of Energy Research, vol. 43, no. 8, pp. 3058–3079, 2019.

[12] Q. H. Wang, K. Kalantar-Zadeh, A. Kis, J. N. Coleman, and M. S. Strano, "Electronics and optoelectronics of two-dimensional transition metal dichalcogenides," Nature Nanotechnology, vol. 7, no. 11, pp. 699–712, 2012.

[13] R. Dai, Y. Wang, J. Wang, and X. Deng, "Metal–organic-compound-modified mos2 with enhanced solubility for high-performance perovskite solar cells," Chem. Sus. Chem., vol. 10, no. 14, pp. 2869–2874, 2017.

[14] I. R. S., X. Xu, W. Yang, F. Yang, L. Hou, and Y. Li, "Highly active and reflective mos2 counter electrode for enhancement of photovoltaic efficiency of dye sensitized solar cells," Electrochimica Acta, vol. 212, pp. 614–620, 2016.

[15] P. Atkins and R. Friedman, Molecular quantum mechanics. New York: Oxford University Press, 4th ed. ed., 2005.

[16] A. R. Leach, Molecular Modelling. Harlow: Prentice Hall, 2nd ed., 2001.

[17] P. Hohenberg and W. Kohn, "Inhomogeneous electron gas," Phys. Rev., vol. 136, pp. B864–B871, Nov 1964.

[18] W. Kohn and L. J. Sham, "Self-consistent equations including exchange and correlation effects," Phys. Rev., vol. 140, pp. A1133–A1138, Nov 1965.

[19] R. O. Jones and O. Gunnarsson, "The density functional formalism, its applications and prospects," Rev. Mod. Phys., vol. 61, pp. 689–746, Jul 1989.

[20] W. Kohn, A. D. Becke, and R. G. Parr, "Density functional theory of electronic structure," The Journal of Physical Chemistry, vol. 100, no. 31, pp. 12974–12980, 1996.

[21] J. P. Perdew, K. Burke, and M. Ernzerhof, "Generalized gradient approximation made simple," Phys. Rev. Lett., vol. 77, pp. 3865–3868, October 1996.

[22] J. P. Perdew, K. Burke, and Y. Wang, "Generalized gradient approximation for the exchange-correlation hole of a many-electron system," Phys. Rev. B, vol. 54, pp. 16533–16539, Dec 1996.

[23] A. D. Becke, "Density-functional thermochemistry. v. systematic optimization of exchange-correlation functionals," The Journal of Chemical Physics, vol. 107, no. 20, pp. 8554–8560, 1997.

[24] C. Kittel, Introduction to solid state physics. Hoboken, NJ: Wiley, 8th ed., 2005.

[25] R. P. Feynman, "Forces in molecules," Phys. Rev., vol. 56, pp. 340–343, Aug 1939.

[26] X. Gonze, G.-M. Rignanese, M. Verstraete, J.-M. Beuken, Y. Pouillon, R. Caracas, F. Jollet, M. Torrent, G. Zerah, M. Mikami, P. Ghosez, M. Veithen, J.-Y. Raty, V. Olevano, F. Bruneval, L. Reining, R. Godby, G. Onida, and D. H. D.C. Allan, "A brief introduction to the ABINIT software package," Zeitschrift für Kristallographie - Crystalline Materials, vol. 220, pp. 558–562, January 2005.

[27] M. Torrent, F. Jollet, F. Bottin, G. Zérah, and X. Gonze, "Implementation of the projector augmented-wave method in the ABINIT code: Application to the study of iron under pressure," Computational Materials Science, vol. 42, pp. 337–351, April 2008.

[28] X. Gonze, B. Amadon, P.-M. Anglade, J.-M. Beuken, F. Bottin, P. Boulanger, F. Bruneval, D. Caliste, R. Caracas, M. Côté, T. Deutsch, L. Genovese, P. Ghosez, M. Giantomassi, S. Goedecker, D. Hamann, P. Hermet, F. Jollet, G. Jomard, S. Leroux, M. Mancini, S. Mazevet, M. Oliveira, G. Onida, Y. Pouillon, T. Rangel, G.-M. Rignanese, D. Sangalli, R. Shaltaf, M. Torrent, M. Verstraete, G. Zerah, and J. Zwanziger, "ABINIT: First-principles approach to material and nanosystem properties," Comput. Phys. Commun., vol. 180, pp. 2582–2615, December 2009.

[29] X. Gonze, F. Jollet, F. Abreu Araujo, D. Adams, B. Amadon, T. Applencourt, C. Audouze, J.-M. Beuken, J. Bieder, A. Bokhanchuk, E. Bousquet, F. Bruneval, D. Caliste, M. Côté, F. Dahm, F. Da Pieve, M. Delaveau, M. Di Gennaro, B. Dorado, C. Espejo, G. Geneste, L. Genovese, A. Gerossier, M. Giantomassi, Y. Gillet, D. Hamann, L. He, G. Jomard, J. Laflamme Janssen, S. Le Roux, A. Levitt, A. Lherbier, F. Liu, I. Lukačević, A. Martin, C. Martins, M. Oliveira, S. Poncé, Y. Pouillon, T. Rangel, G.-M. Rignanese, A. Romero, B. Rousseau, O. Rubel, A. Shukri, M. Stankovski, M. Torrent, M. Van Setten, B. Van Troeye, M. Verstraete, D. Waroquiers, J. Wiktor, B. Xu, A. Zhou, and J. Zwanziger, "Recent developments in the ABINIT software package," Comput. Phys. Commun., vol. 205, pp. 106–131, August 2016.

[30] A. K. Geim and I. V. Grigorieva, "Van der waals heterostructures," Nature, vol. 499, no. 7459, pp. 419–425, 2013.

[31] K. S. Novoselov, D. Jiang, F. Schedin, T. J. Booth, V. V. Khotkevich, S. V. Morozov, and A. K. Geim, "Two-dimensional atomic crystals," Proceedings of the National Academy of Sciences, vol. 102, no. 30, pp. 10451–10453, 2005.

[32] B. Schönfeld, J. J. Huang, and S. C. Moss, "Anisotropic mean-square displacements (msd) in single-crystals of 2h- and 3r-mos2," Acta Crystallogr. B, vol. 39, no. 4, pp. 404–407, 1983.

[33] V. Kalikhman Inorg. Mater., vol. 19, no. 7, pp. 957–962, 1983.

[34] L. Brixner, "Preparation and properties of the single crystalline ab2-type selenides and tellurides of niobium, tantalum, molybdenum and tungsten," J. Inorg. Nucl. Chem., vol. 24, no. 3, pp. 257 – 263, 1962.

[35] W. Schutte, J. D. Boer, and F. Jellinek, "Crystal structures of tungsten disulfide and diselenide," J. Solid State Chem., vol. 70, no. 2, pp. 207 – 209, 1987.

[36] V. L. Kalikhman Neorganicheskie Materialy, vol. 19, no. 7, pp. 1060 – 1065, 1983.

[37] A. A. Yanaki and V. A. Obolonchik Inorg. Mater., vol. 9, no. 12, pp. 1855–1858, 1973.

[38] H. J. Monkhorst and J. D. Pack, "Special points for brillouin-zone integrations," Phys. Rev. B, vol. 13, pp. 5188–5192, Jun 1976.

[39] S. Grimme, J. Antony, S. Ehrlich, and H. Krieg, "A consistent and accurate ab initio parametrization of density functional dispersion correction (DFT-d) for the 94 elements h-pu," The Journal of Chemical Physics, vol. 132, p. 154104, April 2010.

[40] A. D. Becke and E. R. Johnson, "A simple effective potential for exchange," The Journal of Chemical Physics, vol. 124, no. 22, p. 221101, 2006.

ZADÁNÍ BAKALÁŘSKÉ PRÁCE

I. OSOBNÍ A STUDIJNÍ ÚDAJE

Příjmení: **Hulec** Jméno: **Marek** Osobní číslo: **484281**

Fakulta/ústav: **Fakulta elektrotechnická**

Zadávající katedra/ústav: **Katedra elektromagnetického pole**

Studijní program: **Elektronika a komunikace**

II. ÚDAJE K BAKALÁŘSKÉ PRÁCI

Název bakalářské práce:

Kvantově-mechanická studie elektronických vlastností systémů odvozených od dichalkogenidů přechodných kovů

Název bakalářské práce anglicky:

Quantum mechanical study on the electronic properties of systems derived from transition metal dichalcogenides

Pokyny pro vypracování:

Seznam doporučené literatury:

[1] Peter Atkins and Ronald Friedman - Molecular Quantum Mechanics (Fifth Edition) - New York, USA, 2011
[2] Charles Kittel - Introduction to Solid State Physics (Eigth Edition) - New Delhi, India. 2005
[3] M. Z. Iqbal, et al. International Journal of Energy Research 43, 3058 (2019), DOI 10.1002/er.4375
[4] C. M. Went et al. Science Advances 5, eaax6061, 2019, DOI 10.1126/sciadv.aax6061

Jméno a pracoviště vedoucí(ho) bakalářské práce:

Antonio Cammarata, Ph.D., katedra řídicí techniky FEL

Jméno a pracoviště druhé(ho) vedoucí(ho) nebo konzultanta(ky) bakalářské práce:

Datum zadání bakalářské práce: **29.01.2021** Termín odevzdání bakalářské práce: _____

Platnost zadání bakalářské práce: **30.09.2022**

Antonio Cammarata, Ph.D.		prof. Mgr. Petr Páta, Ph.D.
podpis vedoucí(ho) práce	podpis vedoucí(ho) ústavu/katedry	podpis děkana(ky)

III. PŘEVZETÍ ZADÁNÍ

Student bere na vědomí, že je povinen vypracovat bakalářskou práci samostatně, bez cizí pomoci, s výjimkou poskytnutých konzultací. Seznam použité literatury, jiných pramenů a jmen konzultantů je třeba uvést v bakalářské práci.

. _____ _____

Datum převzetí zadání Podpis studenta